universität wien

MASTERARBEIT / MASTER'S THESIS

Titel der Masterarbeit / Title of the Master's Thesis

„Polyphase deformation during subduction and exhumation of the Almyropotamos Window, Evia, Greece“

verfasst von / submitted by

Manuel Kling, BSc

angestrebter akademischer Grad / in partial fulfilment of the requirements for the degree of

Master of Science (MSc)

Wien, 2022 / Vienna, 2022

Studienkennzahl lt. Studienblatt / degree programme code as it appears on the student record sheet:	UA 066 815
Studienrichtung lt. Studienblatt / degree programme as it appears on the student record sheet:	Masterstudium Erdwissenschaften UG2002
Betreut von / Supervisor:	Univ. Prof. Mag. Dr. Bernhard Grasemann

Erklärung

- dass ich die vorliegende Masterarbeit selbstständig verfasst, andere als die angegebenen Quellen und Hilfsmittel nicht benutzt und mich auch sonst keiner unerlaubter Hilfe bedient habe,
- dass ich dieses Masterarbeitsthema bisher weder im In- noch im Ausland in irgendeiner Form als Prüfungsarbeit vorgelegt habe
- und dass diese Arbeit mit der vom Begutachter beurteilten Arbeit vollständig übereinstimmt.

Wien, am 22.12.2022

Acknowledgements

Viele Menschen haben dazu beigetragen, dass ich diese Arbeit abschließen kann. Zunächst möchte ich mich bei Bernhard Grasemann für das Ermöglichen dieser Arbeit bedanken. Für dein offenes Ohr und für die Hilfe bei jeglichen Fragen fachlicher Natur bin ich dir sehr dankbar. Der Aufenthalt in Evia und die gemeinsamem geologischen Exkursionen haben zu meinem heutigen Wissensstand wesentlich beigetragen.
Für die moralische Unterstützung möchte ich mich bei meinen Eltern, Piroska und Christian, und bei meinem Bruder Patrick bedanken. Ihr seid immer an meiner Seite gestanden und habt bewirkt, dass dieses Arbeit auch zu ihrem Abschluss kommt.
Einen ganz speziellen Dank möchte ich meiner Freundin Josefine ausdrücken, die während der ganzen Zeit bedingungslos bei den Höhen und Tiefen dabei war und mir immer Mut gemacht hat die Arbeit zu schaffen.
Meinen Jungs von den Bayreuthern und Hellenen, insbesondere meinen lieben Leibbursch Konstantin möchte ich von ganzem Herzen für den Beistand über die letzten Jahre danken. Ihr habt mein Akademikerherz wie kein anderer befeuert.
Weiters möchte ich in diesem Kontext Jörg Waniek danken. Ohne seine Unterstützung wäre ich heute kein Geologe. Das werde ich nie vergessen.
Meinen Freunden, Kommilitonen und Arbeitskollegen gebührt mein größter Dank für die ständige seelische Unterstützung.

Abstract

The Almyropotamos Window is a tectonic window located in the southern part of the island of Evia, Greece. Evia, as part of the Aegean Sea, forms a geological link between units belonging to the Cycladic Massif in the south and units of the Internal Hellenides in the north. The Cycladic Massif is a nappe stack whose units were juxtaposed during the subduction of the African continent. Three units can be distinguished: (1) The Uppermost Unit which is exposed in the north of the island and has not undergone metamorphism, (2) the allochthonous Cycladic Blueschist Unit(CBU) which has significantly higher metamorphic conditions than the (3) Basal Unit or locally called Almyropotamos Unit which is exposed in the Almyropotamos Window.

The Almyroptomos Window is dominated by two lithologies: marbles whose protoliths were formed during the Mesozoic topped by an Eocene metaflysch deposited over the marbles.

In the course of this master thesis an extensive mapping, as well as a structural geological analysis of the Almyropotamos Windows was carried out. The structural geological analysis includes the recording of terrain data, the collection of samples with subsequent microstructural evaluation, measurements of XYZ-data based on marble pebbles in flysch zones, and statistical evaluations of a fracture corridor using the Matlab toolbox FracPaQ. In addition to a detailed geological map, which focuses mainly on structural geological content, two profiles are presented. Furthermore, a geodynamic model was created to summarize the formation history and main deformation events of the Almyropotamos tectonic window.

Subduction and extension with subsequent exhumation are the processes that have significantly contributed to the polyphase deformation of the cycladic units and subsequently to the present expression of the Almyroptomaos window. Based on the observations and measurements from the field, as well as the evaluation of various rock samples, 4 deformation phases can be distinguished. With D(1-3) all deformation phases belonging to the ductile to brittle-ductile regime are described. During a first fully ductile phase D1 occurred whereby rocks of the Almyroptamos Unit were subducted and deformed. Subduction resulted in the formation of isoclinal folds with fold axes oriented E-W parallel to the stretching lineation. During a second fully ductile phase, described as D2, another folding event occurs during which the rocks of the Almyropotamos Unit underwent E-vergent folding. D3 describes a brittle-ductile phase in which old shear zones such as the so-called Buffalo Shearzone are reactivated and the rocks of the Almyropotamos Windows are stretched in a top-W direction. While D1 is attributed to the subduction of the Almyropotamos Unit, D2 and

D3 already belong to the exhumation phase of the cycladic units under the Northern Cycladic Detachment System (NCDS). D4 describes a final deformation phase in which top-E directed cataclasites or shear zones are formed across the area and occurs as the coolest and last event in the brittle regime.

For D1 and D2, metamorphic conditions of about 8-10 kbar and 400 °C are established based on the evaluation of the literature and existing fieldwork, corresponding to the lower blueschist facies. For D3, the metamorphic conditions are about 4 - 7 kbar and 300 - 400 °C and can thus be assigned to the greenschist facies. The observed metamorphic conditions are consistent with other research.

The results of the XYZ-measurements vary depending on the location in the area. For example, elongated pebbles were mainly observed at the edge of the area and in the center, but they were additionally strongly flattened in shear zones such as the Buffalo Shear Zone. Overall, the measurements result in two trends with increasing strain, one in the field of apparent constriction and one in the field of apparent flattening.

All observed and measured structures were presented in a 3D synoptical diagram according to their origin and after classification in the geodynamic model.

Zusammenfassung

Das Almyropotamos Window ist ein tektonisches Fenster welches sich im südlichen Teil der Insel Evia, Griechenland, befindet. Evia als Teil des ägäischen Meeres bildet eine geologische Verbindung zwischen Einheiten, die dem kykladischen Massiv im Süden angehören und Einheiten der Internen Helleniden im Norden. Das kykladische Massiv ist ein Deckenstapel, dessen Einheiten während der Subduktion des afrikanischen Kontinents nebeneinander abgelagert wurden. Es können drei Einheiten unterschieden werden: (1) Die Uppermost Unit, welche im Norden der Insel aufgeschlossen ist und keine Metamorphose erfahren hat, (2) die Cycladic Blueschist Unit (CBU) hat deutlich höhere Metamorphosekonditionen als die (3) Basal Unit bzw. Almyropotamos Unit genannt welche im Almyropotamos Window aufgeschlossen ist.

Das Almyroptomos Window wird von zwei Lithologien bestimmt: zum einen Marmore dessen Protolithe während des Mesozoikums gebildet wurden und zum anderen im Eozän gebildete Metaflysche die über den Marmoren abgelagert wurden.

Im Zuge dieser Masterarbeit wurde eine umfangreiche Kartierung sowie eine strukturgeologische Analyse des Almyropotamos Windows durchgeführt. Zur strukturgeologischen Analyse zählen die Aufnahme von Geländedaten, das Sammeln von Proben mit anschließender mikrostruktureller Auswertung, Messungen von XYZ-Daten anhand von Marmorpebbles in Flyschzonen sowie statistische Auswertungen eines "fracture"-Korridors mittels der Matlab-Erweiterung FracPaQ. Neben einer detaillierten geologischen Karte, die sich vor allem auf struktugeologische Inhalte fokussiert, werden zusätzlich zwei Profile präsentiert. Weiters wurde ein geodynamisches Modell erstellt, welches die Bildungsgeschichte und Hauptdeformationsereignisse des tektonischen Fensters von Almyropotamos zusammenfassen soll.

Subduktion und Extension mit anschließender Exhumation sind die Prozesse, die wesentlich zur polyphasen Deformation der kykladischen Einheiten und in weiterführender Folge zur heutigen Ausprägung des Almyroptomaos Windows beigetragen haben. Basierend auf den Beobachtungen und Messungen aus dem Feld, sowie der Auswertung diverser Gesteinsproben können 4 Deformationsphasen unterschieden werden. Mit D1 bis D3 werden alle Deformationsphasen die dem duktilen bis zu brüchig-duktilem Regime angehören, beschrieben. Während D1 kam es zu einer ersten vollduktilen Phase wobei Gesteine der Almyroptamos Unit subduziert und stukturell umgewandelt wurden. Durch die Subduktion kam es zur Ausbildung von Isoklinalfalten dessen Faltenachsen E-W streichen und parallel zur Streckungslineation stehen. Während einer zweiten vollduktilen Phase, die als D2 beschrieben wird, kommt es zu einem weiteren Verfaltungsevent bei der die Gesteine der

Almyropotamos Unit eine E-vergente Verfaltung erfuhren. D3 beschreibt eine brüchig-duktile Phase bei der alte Scherzonen wie die sogennanten Buffalo Shearzone reaktiviert werden und die Gesteine des Almyropotamos Windows Top-W gerichtet gestreckt werden. Während D1 der Subduktion der Almyropotamos Unit zugeschrieben wird, zählen D2 und D3 bereits zur Exhumationsphase der kykladischen Einheiten unter dem Northern Cycladic Detachment System (NCDS). Bei der letzten Deformationsphase, die als D4 beschrieben wird, kommt es zur Ausbildung von Top-E gerichteten Kataklasiten bzw. Scherzonen die über das Gebiet verteilt sind. Dieses D4 Event tritt als kühlstes und letztes auf.

Für D1 und D2 werden anhand der Auswertung der Literatur und vergangener Arbeiten metamorphe Konditionen von ca. 8 - 10 kbar und 350 °C festgelegt, was der unteren Blauschieferfazies entspricht. Bei D3 betragen die metamorphen Konditionen ca. 4 - 7 kbar und 300 - 400 °C und können somit der Grünschieferfazies zugeordnet werden. Die beobachteten metamorphen Konditionen stimmen mit anderen Forschungsarbeiten überein.

Die Ergebnisse der XYZ-Messungen sind je nach Lage im Gebiet unterschiedlich. So wurden am Rand des Gebietes und im Zentrum vor allem elongierte Pebbles beobachtet, jedoch waren diese in Scherzonen wie der Buffalo Shearzone zusätzlich stark geplättet. Insgesamt ergeben die Messungen zwei Trends mit steigender Beanspruchung, einen zusammendrückenden Trend ("constriction") und einen verflachenden Trend ("flattening").

Alle beobachteten und gemessenen Strukturen werden ihrer Enstehung entsprechend und nach Einordung in das geodynamische Modell in einem 3-dimensionalem synoptischen Diagramm präsentiert.

Contents

1. Introduction

The Mediterranean region as we know it today is the product of a long and complex interplay of diverse processes that need to be studied in order to discuss the exact history of its formation. As part of the Mediterranean Sea, the Aegean represents a crucial part that holds many geodynamic processes in its rocks (Jolivet and Brun, 2010). To connect these processes and to understand them, metamorphic rocks are an essential component. Through their physical properties (rheology, density, fluid transport capacity), they hold information over very long periods of time, helping to develop geodynamic models (Burov et al., 2014). The collision of the African plate with the Eurasian and various microplates gave the starting signal for a long series of processes that were set in motion. Two main processes are subduction of continental/oceanic crust and exhumation of these buried parts (Jolivet and Brun, 2010).

On the island of Evia there is the opportunity to gain insight into these processes, because it is the link between the Cyclades in the south of the Aegean and the internal Hellenides in the north (Ring et al., 2007). In the south of the island, rocks of the Cycladic Blueschist Unit (CBU) are exposed, which were thrust during the subduction of the African plate over rocks that were structurally under the Blueschist Unit. These rocks belong to the Basal Unit, locally also called Almyroptamos Unit (AU), and are exposed in a tectonic window by exhumation processes combined with erosion (Xypolias et al., 2003).

Geochronological data and research results from recent years have established two metamorphic events that contribute significantly to the formation of the present situation on Evia and the Aegean Region: a (1) high-pressure phase (blueschist-eclogite facies, 15 kbar 450 - 500 degrees) that occurred during the end of the Cretaceous to the middle Eocene followed by a (2) low-pressure phase (greenschist amphibolite facies, 4 - 7 kbar, 440 - 470 degrees) (Shaked et al., 2000) that occurred during the Oligocene/Miocene. Relics of this polyphase deformation can be studied in the Almyropotamos tectonic window.

1. Introduction

Although polyphase deformation on Evia has been established by geochronological data, the geodynamic evolution of Evia remains controversial to this day. Xypolias and Gerogiannis point to a bivergent geometry (SW-NE direction) of the kinematics during the subduction-exhumation cycle of the Cyclades and Hellenides (Gerogiannis and Xypolias, 2017; Gerogiannis et al., 2021). This is contrasted with an univergent model (Grasemann et al., 2018; Ring et al., 2010) in which the Cycladic and Hellenides units were resurfaced along a subduction channel (Hellenic subduction channel) and the formation of a back arc extension by the slab retreat of the African plate and evolution of the Northern Cycladic Detachment System (NCDS) (Jolivet and Brun, 2010; Jolivet et al., 2010).

The tectonic window of Evia provides information that contributes to a better understanding of the evolution of Evia and the Aegean Region. A new map with profiles was created to better understand the complex tectonic window of Evia from a geological point of view. Through field work, the analysis of structural geological data and microstructural observations, a geodynamic model is presented which will contribute to the understanding of the complex deformation history of the Aegean region.

2. Background

2.1. The Aegean Sea and its diverse structure

Several studies show the complexity of the geological framework of the Aegean Sea. Based on defining the rock types stratigraphy, tectonometamorphic history and pre-orogenic paleogeography, five tectonic zones from Top to Bottom could be distinguished as:
(A) the Internal Zone, (B) the Vardar-Izmir-Ankara-Zone, (C) the Pelagonian Zone,
(D) the Cycladic Zone and (E) the External Hellenides (Ring et al., 2010), which are shown in Figure 1.
However, the creation of these tectonic nappes is the result of complex geodynamic processes such as oceanic and continental subduction, mountain building, high pressure, and low-temperature metamorphism, backarc extension, post-orogenic collapse, metamorphic-core complexes, and gneiss domes, which are described in several studies (Jolivet and Brun, 2010). The Aegean sea as it can be seen in the present days started to form in the Oligocene and can be classified as a mediterranean back-arc basin (Jolivet and Brun, 2010). Its evolution is deeply connected with the active kinematics of two independent components: (1) the retreat of the subducting African plate and (2) the westward motion of the Anatolian Plate along the North Anatolian Fault (Jolivet, 2001; Jackson, 1994).
Since the cretaceous magmatic rock formation has emplaced in the Aegean region starting with a magmatic arc in the Balkan region (Janković, 1997; von Quadt et al., 2005) with further migration of the arc southwards to its present-day location since the Oligocene (Fytikas et al., 1984; Pe-Piper and Piper, 2002, 2006, 2007). Magmatism can also be recognized near the NW part of Evia linked with the propagation of the North Anatolian Fault. The main cause of volcanic arc formation is subduction (Jolivet and Brun, 2010).

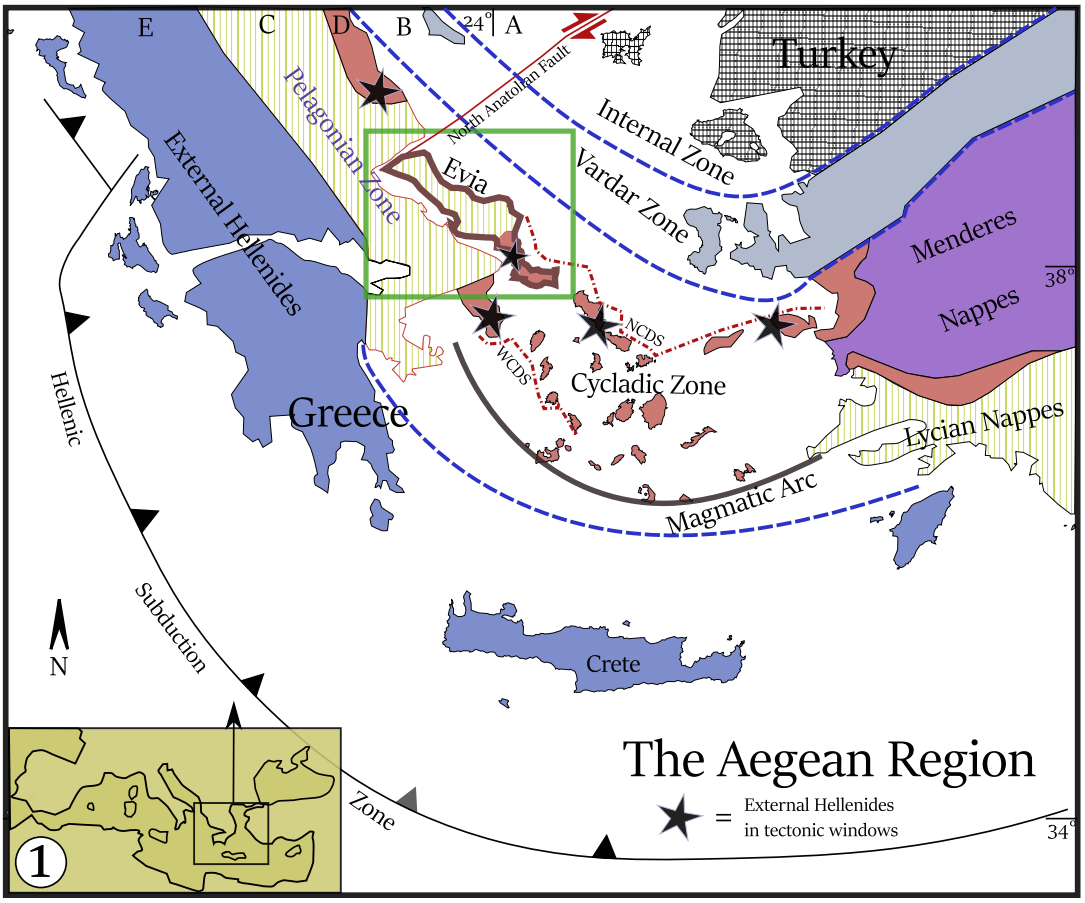

Figure 1.: The Aegean region

Generalized tectonic map of the Aeagean region showing major tectonic units (A-E) and the present location of the Hellenic Subduction Zone. The island of Evia is marked with the green box, where the study area is located. The Basal Unit crops out in different tectonic windows, marked with stars. The map is modified after (Ring et al., 2010).

The Cyclades, where the study area is located, were strongly affected by post-orogenic extension linked to the Aegean extension and the formation of the Hellenides (Jolivet et al., 1994; Avigad et al., 1997; Jolivet, 2003) linked to syn-orogenic exhumation. Due to this strong extension, metamorphic rocks crop out on the cycladic islands. Furthermore, palaeomagnetic rotations are recorded throughout the Aegean Sea (Kissel et al., 1995; Haubold et al., 1997). They appear mostly clockwise but in the cycladic massive the rotation seems more complex.

Linked with the subduction of the African Plate three major processes can be described overall for the whole Aegean region: (1) Compression, (2) Extension and (3) Magmatism. These processes can occure alone but mostly in combination and beginning with compression due to the beginning of the subduction followed by extension through slab retreat. In some

regions of the Aegean sea magmatism occurs before the subduction but is mostly connected with extension (Jolivet and Brun, 2010).
In the Cyclades an overall compression under High Pressure - Low Temperature (HP-LT) conditions is recorded beginning with Eocene. Under these conditions the HP-LT rocks of the CBU formed (Ring et al., 1999; Gessner et al., 2001). With the beginning of the Oligocene the regime switched to an extensional regime where the exhumation of the cycladic island took place, contemporary with magmatic arc formation under high temperature – low pressure (LP-HT) conditions (Jolivet and Brun, 2010).

2.2. Geology of Evia

Evia, as part of the westernmost area of the Aegean sea, is placed in the middle between a complex stack of tectonic nappes, connecting external and volcanic arc regions in the southern aeagean sea with units belonging to an internal, continental regime in the north (Shaked et al., 2000). Three tectonic units are exposed on Evia, (which leads to insights how these units have been formed and which processes and kinematics have been active) which are described from Top to Bottom:

(1) The Uppermost Unit contains Late Cretaceous Amphibolites and Gneisses, Palaeocene Greenschists and marbles and ultramafic rocks (Martha et al., 2016; Aravadinou and Xypolias, 2017).
(2) The Cycladic Blueschist Unit (CBU) comprises Metapelites, marbles, meta-igneous rocks with Mesozoic protolithic ages, which developed in a back-arc setting or passive-rift margin (Okrusch and Bröcker, 1990).
(3) The Basal Unit or locally Almyropotamos Unit (AU) is represented by Mesozoic marbles overlain by tertiary flysch (Avigad et al., 1997; Xypolias et al., 2003).

In difference to (2) and (3) the Uppermost Unit represents the Internal Hellenides, which was slightly/not affected by Eocene HP – Metamorphism (Katzir et al., 2000), whereas both the CBU and Basal Unit belong to the Cycladic Zone. The two main domains of Internal Hellenides and Cycladic Zone are divided by a major thrust contact, which

juxtaposed the tectonically highest (Pelagonian) Unit with the lowest one, the Basal Unit or Almyropotamos Unit. In southern direction of this major thrust, the so called Pelagonian Normal Fault, only rocks of the Cycladic Zone are outcropping (Xypolias et al., 2003).

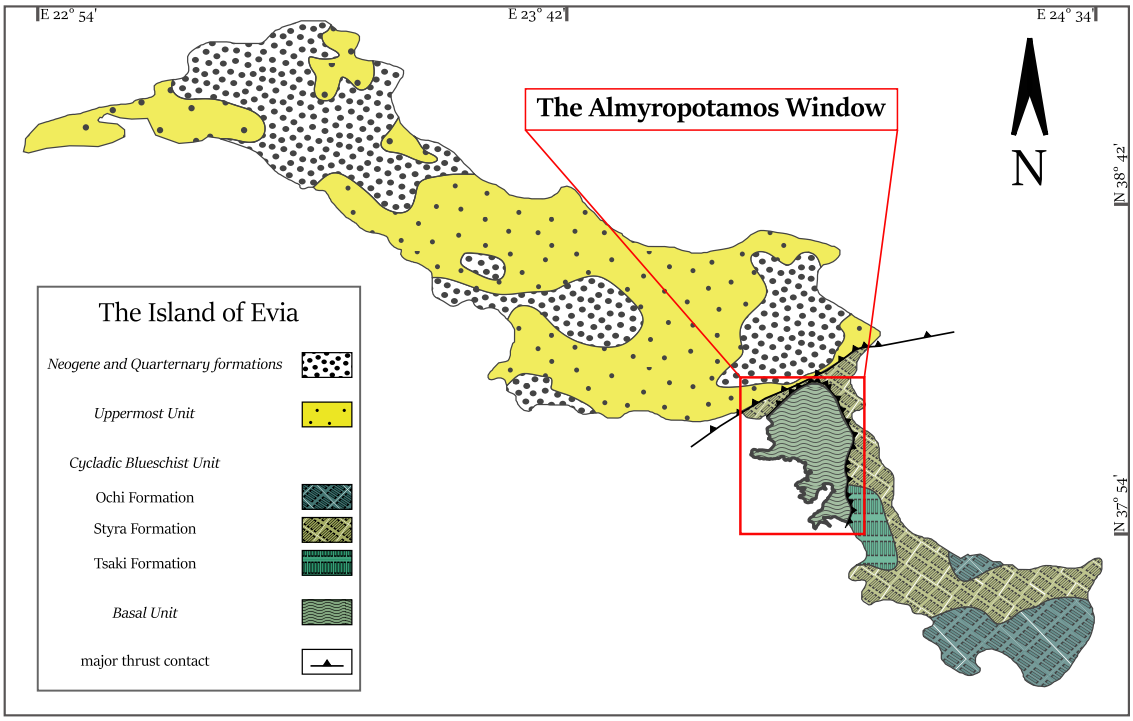

Figure 2.: Map of Evia

Geological Map of the island of Evia showing the three major units of the Cycladic Zone and exact location of the Almyropotamos Window. A major thrust contact seperates the parts of the Pelagonian Unit belonging to the Internal Hellenides from the Cycladic Blueschist Unit (CBU) belonging to the Cycladic Zone. The map is modified after (Shaked et al., 2000)

.

The CBU on Evia (Evia Blueschist Unit =Evia Blueschist Unit) can be subdivided in three nappes from Top to Bottom (Gerogiannis et al., 2021):

(a) The Tsaki-Nappe includes mica – chlorite schists with impure marble intercalations. Outcrops can only be found in the southern/eastern parts of Evia.

(b) The Styra-Nappe contains an impure marble-schist-sequence and can be found in the middle and eastern parts of Evia Island.

(c) The Ochi-Nappe represents a meta-volcano sedimentary sequence. Outcrops are located at the southernmost tip of Evia.

These Nappes underwent two stages of metamorphism, one high-pressure stage showing blueschist to eclogite conditions (15kbar; 400 – 500°C) of Late Creataceous – Middle Eocene age (60 – 70 Ma to 45 – 50 Ma) followed by a lower-pressure stage showing greenschist conditions (4 – 7 kbar; 440 – 470 or 650°C) during Oligocene/Miocene times (Shaked et al., 2000).

2.3. Geology of the Almyropotamos Window

Below the CBU, to the southwest of Evia, the Basal Unit, locally called the Almyropotamos Unit (AU) (Xypolias et al., 2003), is exposed in the form of a tectonic window. The paraautochthonous AU, is attributed to the external Hellenides and consists of a 2km thick series of marbles overlain by a 1500m thick sequence of metaquartzite pelites. The protoliths of these sediments were deposited during Triassic to Eocene time as limestones of a carbonate platform between the Pelagonian and Almyropotamos microcontinents (Xypolias et al., 2003). Two metamorphic events are thought to have contributed to the present-day structure of the Almyropotamos Windows. These events are similar to those seen in the CBU, but the metamorphism was not as strong. The first event D1 which took place at the end of the Eocene/Oligocene (50-45 Ma) under blueschist HP-LT conditions (8-10kbar, 350°C) is followed by a second event D2 at the end of the Oligocene under greenschist facies MP-LT conditions (4-7 kbar, 300 - 400°C) (Shaked et al., 2000). D1 was triggered by subduction of the African plate which caused the CBU to be underthrusted by the AU. Underthrusting and subduction of CBU and AU continued for about 20 Ma years, reaching depths of about 40km (Katzir et al., 2000). Due to the slab retreat of the African plate (Jolivet and Brun, 2010) and the evolution of the Northern Cycladic Detachment System (NCDS) (Jolivet et al., 2010), exhumation processes occurred whereby the AU together with the CBU received a greenschist facies overprint by decompression as previously described (Shaked et al., 2000). In connection with the decompression there is also a backarc extension of the Aegean (Jolivet and Brun, 2010).

3. Methods

Methods used during the work are explained in more detail in the following chapters.

3.1. Mapping and Sampling

Detailed geological fieldwork has been carried out of the Almyropotamos Window in the south of Evia Island. The main interest of the work is to create an exact geological map of the Window including all the lithodemic units and structures which will be shown in the next chapter. The work can be generally divided into 2 parts: The fieldwork that took place on Evia and the evaluation and editing phase. Via remote sensing, the area was analyzed before the field trip to see where possible outcrops could be found in the window. With the support of Locus Mobile Application, waypoints were created to have digital information available. First, a field map was created to mark outcrops and lithologies. The field-measurements were carried out by a Clar-Compass with support from the Rocklogger application. Important field measurements conducted are:

- Foliation
- Lineation
- Axial Plane schistosity
- Brittle and ductile faults
- Fold limbs, fold axis, fold axial plane

After the field work, the acquired map material was digitized and the collected data was incorporated into a database for further use. With the help of the software QGIS, the field map was georeferenced so that a (structural-) geological map with all collected

information from the field can be created. QGIS was also used to create two profiles. Using the qprof-tool, profiles were created using pre-drawn vectors and available Digital Elevation Models (DEM), which could then be further processed in a vector graphics program. The database was created to have the measurements collected and organized and to be able to make specific queries. The measurements could be imported into QGIS via .csv files and stereoplots could be created via usage of the software Stereonet for specific areas and measurement types. Since the database was also linked to the images taken in the field, it was also possible to work on an outcrop-specific basis, since each outcrop point in the database now has all the information.

Since one of the research questions is what the strain conditions were in the area, specific measurements were made on pebbles in the metaflysch. For this purpose, the strain axes of the pebbles were identified in order to determine the aspect ratios of XYZ-axes. In the area, outcrops with pebbles were not always found or the outcrop situation was so poor that the axes could not be determined. Nevertheless, measurements were made distributed over the area. The results were also incorporated into the database and subsequently presented in a Flinn and Nadai diagram.

In order to perform a microstructural analysis, samples were taken distributed over the area. The samples were equally taken from the marble and flysch units. Special attention was paid to contact zones between marble and flysch. The samples were cut and analyzed under a transmitted light microscope after thin section preparation. Care was taken to record the mineral structure, mineral composition, and microstructures. The aim was also to establish correlations between deformation events and microstructures under the microscope. After the analysis of all samples, suitable samples were selected to create photos using a photomicroscope. The photos were processed in a vector graphics program, recognized structures and important information regarding mineral composition as well as deformation events were thus compiled.

From the field data as well as the findings of the microstructure analysis a synoptic was created for a better spatial representation of all structures and lithologies.

3.2. FracPaQ

During the analysis of the research area, remote sensing was used to locate an area in the south of the area that contains conspicuous structures. This is a fracture corridor that runs from the northeast to the southwest. To get an idea of the fracture patterns in the found area a fracture network analysis was performed using the program FracPaQ ("Fracture Pattern Quantification") (Healy et al., 2017). FracPaQ is an open source toolbox available on the internet and written in MATLAB© to quantify fracture patterns. For this purpose, either an image file or a text file containing XY data is loaded into the program, which is then analyzed for self-selected parameters. In this work, a high-resolution image of the fracture corridor was created using Google Earth© and subsequently processed in a vector graphics program CorelDraw©. The fractures were traced via a polygontool and the entire polygons were saved as .svg (Scaled Vector Graphics). FracPaQ recognizes these polygons and creates a map where the fractures are shown as a whole ("traces") but also with their nodes (click points) and segments (between nodes). For this work the found fracture corridor was checked for the connectivity of the fractures, its length distribution, the angular relationships between the fractures, the permeability, the Mohr's fracture criterion and for the normalised slip tendency. The results calculated via MATLAB© could be saved as .jpg or .svg. The results are presented in the Structural Analysis chapter.

4. Lithological Description

In this section the lithologic units of the research area are presented, as well as a detailed geologic map and two profiles. In the Almyropotamos window, two major components of the Basal Unit of the Cycladic Massif are exposed:

- Marbles of the Basal Unit or Almyropotamos Unit (AU) in the local literature (Xypolias et al., 2003) with flysch intercalations.
- Flysch with metacarbonate layers (Shaked et al., 2000).

The marbles of the AU can be divided into two types, on the one hand into the lower marble sequence formed during the Mesozoic (Triassic - Cretaceous) and on the other hand into the upper marble sequence formed at the end of the Mesozoic (Cretaceous - Eocene) (Xypolias et al., 2003). In the research area only the marbles of the upper sequence were exposed. For the sake of clarity, the lithological descriptions are subdivided according to the two main lithologies.

4.1. Marbles of the Almyropotamos Unit

The marbles of the Almyropotamos Unit are proportionally the most represented in the Almyropotamos tectonic window and occur in every area of the research site. The marbles are predominantly gray to white and show different structural expressions depending on the location of the outcrop. The thickness of the marble sequence in the area is up to 600m and the outcrops are more or less very accessible on foot. In the marble macroscopically few other minerals could be recognized, the rock structure shows itself rather monomineralic. The formation of the marbles goes back to the Cretaceous where limestones were deposited in the form of carbonate platforms.

4. Lithological Description

In the course of the collision between the African and Eurasian continents, there was first a compression of the carbonate platform located between the continents with a subsequent extension, whereupon the basal unit with the marbles were exhumed again (Xypolias et al., 2003).

Because of this complex formation history, structures were formed that can be measured and interpreted. The outcrops with the most information are located close to the flysch zones and therefore it can be assumed that the two main lithologies are closely related. In the northwestern, northeastern and southwestern part of the research area, where the flysch zones are also found, an increase in mylonitization of the marble was observed. Indicators of this are the formation of increasingly fine-grained layers, Domino-type boudins (see Figure 3a, (Goscombe et al., 2004)), pinch and swell structures (Fig. 3b), the formation of SCC' structures, shear band boudinages of dolomitic layers and stretching lineations. Slickenfibres were used to support the evaluation of movement directions. Besides the previously mentioned structures, different forms of folding could be seen in cm to m range. Furthermore, based on the fold formation, two types could be distinguished. On the one hand the formation of isoclinal folds (Fig. 3c) and on the other hand the formation of tight to open folds (Fig. 3d). The isoclinal folds form thicked hinges and elongated limbs. In the southern and eastern part the folding could be reconstructed three-dimensionally by measurements of axial plane schistosity. On the peninsula in the west, the outcrop conditions were somewhat worse than in the rest of the area, but some core fold zones could be found. Especially near the coast in the west of the peninsula veins could be found in the marble. The veins were oriented almost perpendicular to each other, along N-S and E-W. Brittle deformation was found by fractures in some areas of the area, but mainly localized in the central zones of the area. The caliche cementation and formation of speleothems and fracture zones of the marble were conspicuous throughout the area.

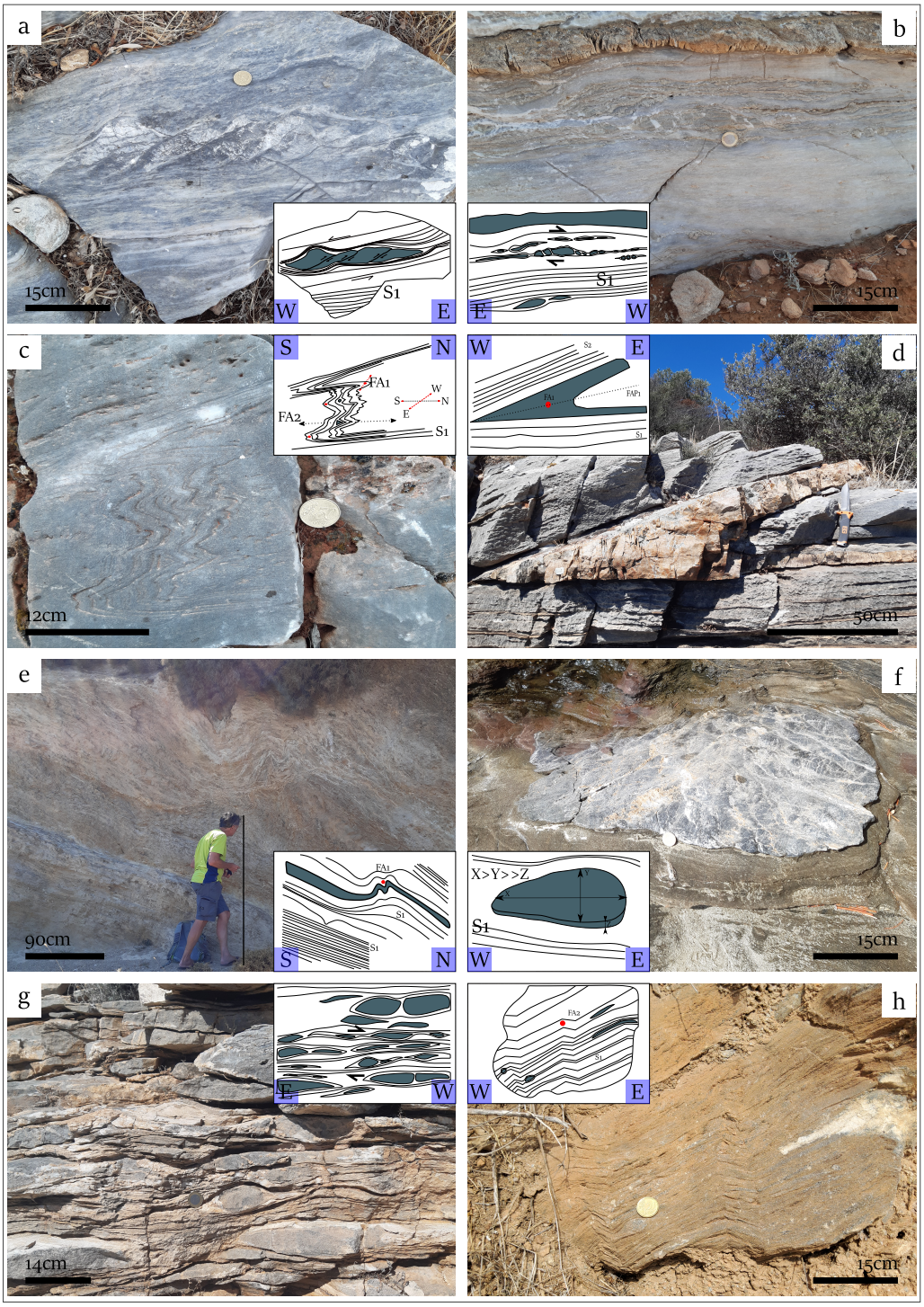

Figure 3.: Pictures and sketches showing geological features on mesoscale.

(a) rotated boudins and pinch and swell structures in marble found in the Buffalo Shearzone. Rotation indicates a westward extension (UTM35 247113/4239257). (b) full ductile pinch and swell structures in marble indicate westward extension under mylonitization of the marble layers (UTM35 240339/4247323). (c) Mushroom type folds indicate two generations of folding. The N-S orientation of one fold generation is estimated belonging to the first ductile stage of D1 (UTM35 248502/4238599). (d) fold with thicked hinges and sharp boundaries. Folding belongs to second stage full ductile deformation D2 with E-vergent folding of all rocks in the study area. S2 has been evolved during later brittle-ductile D3-event (UTM35 240509/4246210). (e) Relicts of N-S striking folds in brittle cataclasites, which have been evolved along E-W (UTM35 249790/4242645). (f) 3D-capture of a marmor pebble, surrounded by metaflysch, where all principle stress axes can be determined. Outcrop is located in the Buffalo Shearzone where most of the strain was localized, indicated by extreme flattening of the pebbles (UTM35 247059/4239242). (g) Boudinaged marmor pebbles in metaflysch showing brittle-ductile westward extension estimated to be deformed during D3 (UTM35 240151/4246031). (h) Kinkfolds as a result of brittle-ductile deformation during D3. Fold Axes are N-S orientated (UTM35 249677/4241443).

4.2. Metaflysch of the Almyropotamos Unit

In contrast to the marble, the flysch zones are much less exposed or not exposed at all. Roughly, two zones can be divided: (1) the coastal flysch zones that run first from west to east and then southward, and (2) flysch zones that run roughly along a north-south axis in the east of the area. The flysch zones can vary greatly in their structural characteristics. For example, there are flysch that are very fine-grained but may also contain rounded marble pebbles (see Fig. 3g). The marble pebbles can be of different sizes, but they can be confined up to a few cm to m. During mapping, these flysch zones were classified as metaconglomerate because of the roundedness of the marble clasts. As the next stage, there were flysch zones without rounded components with very fine layers of siliciclastic and carbonate minerals. Where strain was particularly strongly localized, cataclastic zones could be found. A valuable indicator to find good outcrops was the local vegetation. Since in the Almyropotamos Window otherwise only marble is exposed and this offers only little space for soil and root formation due to its resistance to weathering, the vegetation recedes to areas with good soil formation. Via remote sensing, very dense areas of vegetation could be located and in the field this auxiliary method has proven to be very useful and reliable. The flysch has mostly brown to yellow colors and is characterized by its fine graininess. Structures could be recognized in almost all outcrops, but there were areas, such as in the northeast, where due to too much vegetation a clear lithological address and thus also a structural geological analysis was not possible. Structures ranged from ductile, brittle-ductile to brittle. Typical structures were SCC'-fabrics and folding structures. In some outcrops, foliations and lineations could be measured. Besides stretching lineations, crenulation lineations could be identified helping to spatially analyse the fold data. Another important method in this work was the evaluation of axial ratios from the marble pebbles. These were found in several outcrop, some had even a three-dimensional access to gain measurements of all three strain axes (Fig. 3f). The marble pebbles could be elongated, flattened or dynamically deformed, in any case with this method on the one hand the deformation regime and on the other hand the degree of strain could be estimated. Fold structures could be divided into: (1) very tight isoclinal folds trending E-W, (2) tight to open folds trending N-S and (3) brittle-ductile formed kinkfolds (Fig. 3h). Cataclastic zones

could be identified in the south and in the center of the research area. These cataclastic zones contained hardly any marble pebbles which can be attributed to strong strain (Fig. 3e). Structural measurements showed consistent values in the eastern area along the north-south oriented flysch zone, whereas measurements in the flysch zones on the peninsula in the western area did not always yield coherent results (see subsection 5.1.3).

4.3. Map and Profiles

In the following section, a new geological map is presented with two profiles.

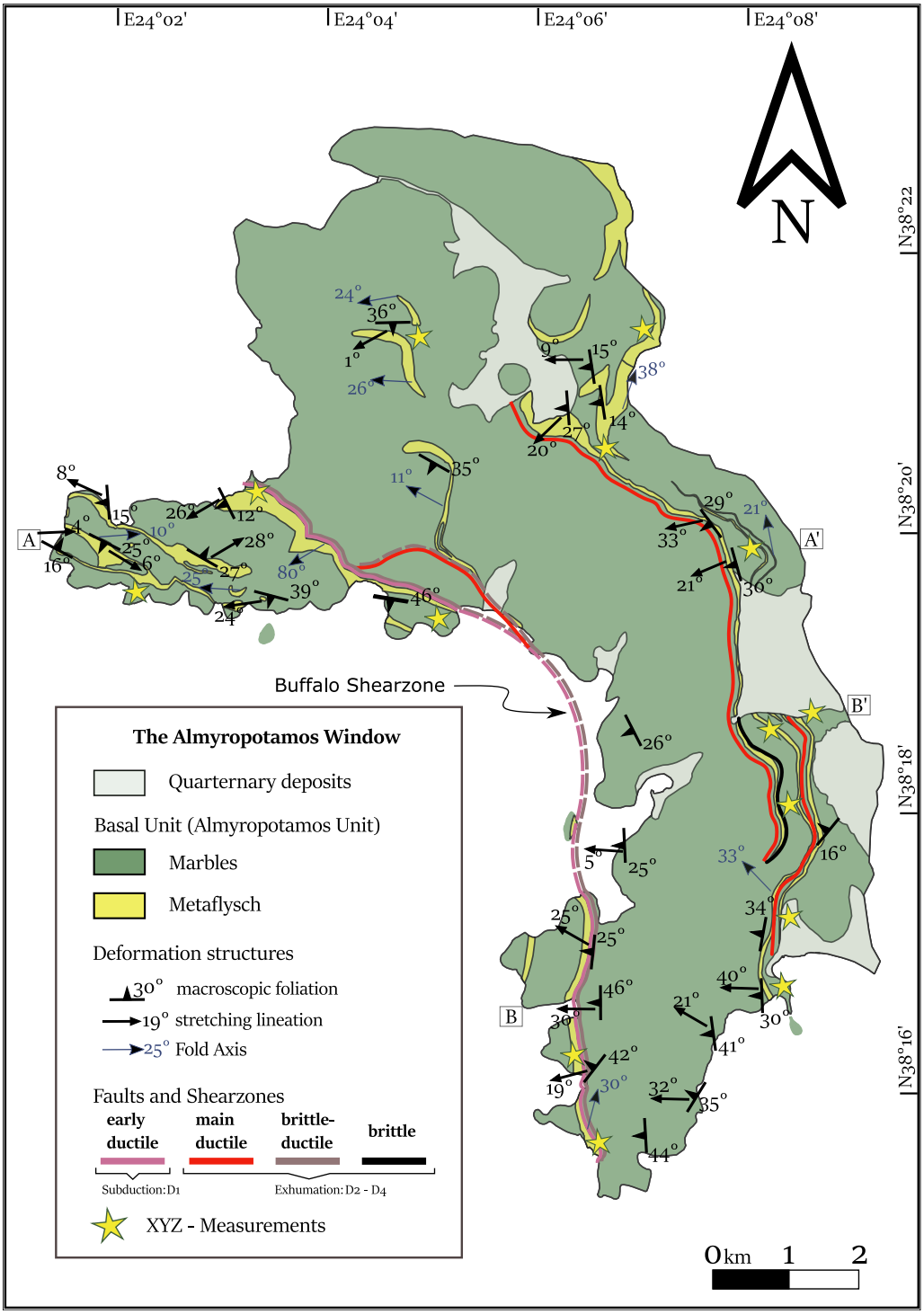

Figure 4.: Map of the study area

Geological map of the study area with major lithologies and large-scale structures based on mapping and outcrop observations. Different deformation stages are indicated by coloured lines.

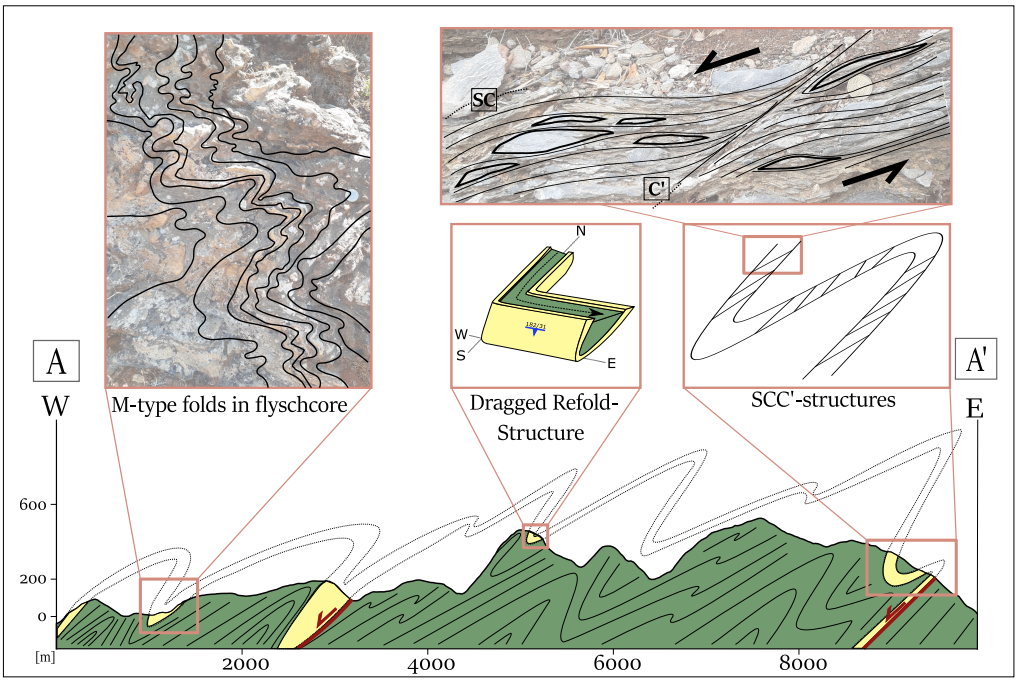

Figure 5.: Northern Cross Section of the study area.

See Figure 4 for exact location in the study area. Note the E-vergent folding of the whole area due to late D2 deformation. Outcrop (a) shows folding of higher order (UTM35 241361/4246620), (b) shows a fold-core dragged into the Buffalo shearzone (UTM35 247509/4250987) and (c) shows SCC' structures indicating top-to-the-W extension (UTM35 247074/4239247).

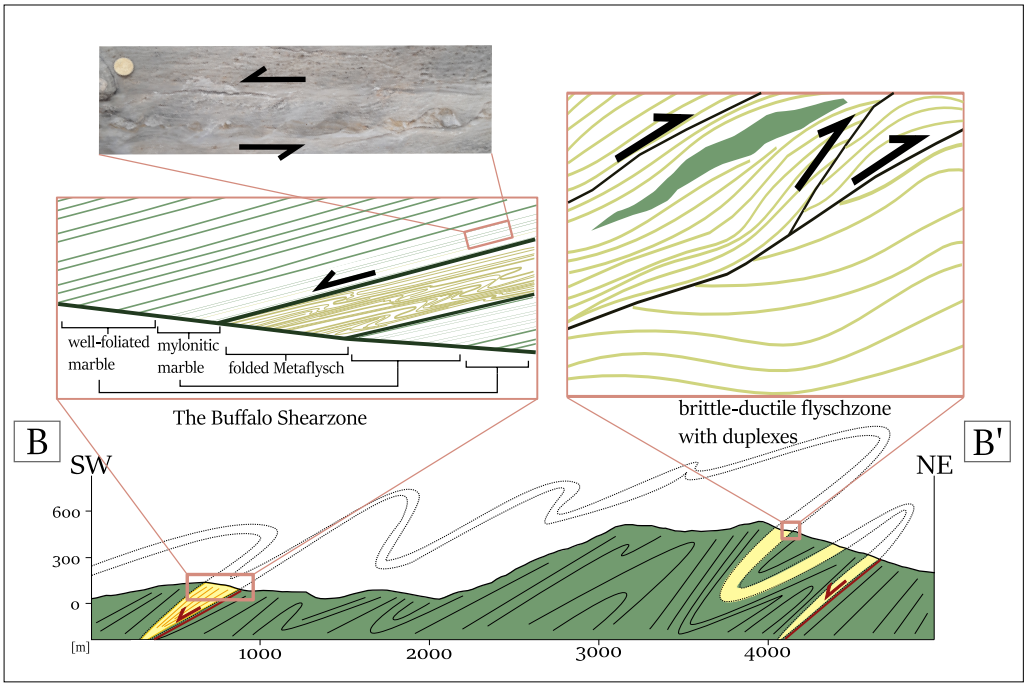

Figure 6.: Southern Cross Section of the study area.

Note the Shearzone on the left in yellow colours which is the Buffalo Shearzone (can also be seen in figure 5). It has been fully ductile in the early stages of D1 (see mylonitization in shearzone-core) and has been reactivated during brittle-ductile stage of D3. Outcrops (a) showing stronger mylonitization towards shearzones (UTM35 247113/4239257) and (b) showing brittle-ductile duplex structures (UTM35 249726/4242881).

5. Structural Analysis

In the following chapter the results of the field work and the microstructural analysis are presented. All structures that have been found and analyzed micro- or macroscopically are presented in a 3D synoptic at the end of the chapter.

5.1. Outcrop Observations

Two main events have been recognized by various works that are significantly involved in the present-day formation of the area and, consequently, in the formation of the local rocks (Shaked et al., 2000): (D1): A compression of rock units related event on Evia due to subduction of the African plate beneath the Eurasian plate at the end of the Eocene/Oligocene under blueschist conditions (HP-LT). (D2): Extension and exhumation of rock units by the slab reatreat of the African plate (Jolivet and Brun, 2010) and the evolution of the NCDS (Jolivet et al., 2010) under greenschist facies conditions (MP-LT) between Oligocene and Miocene.

Pre-D1 structures were not found and measured in the area. It is possible, that to S1 assigned foliation can be the original bedding. To better classify the observed structures to the deformation events, the area was divided into three parts: the (1) southern, (2) central and northern, and (3) western parts.

5.1.1. Southern Area

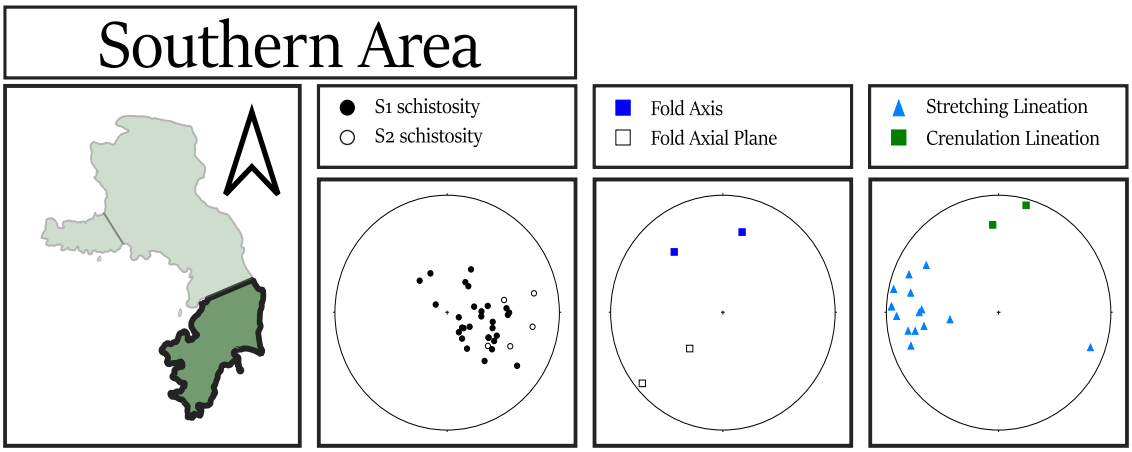

Figure 7.: The Southern area.

Measured structural data of the most important geological parameters.The Southern area was usefull to study the evolution of the Buffalo-Shearzone and the second stage of full-ductile D1 deformation.

The southern area is characterized by a N-S trending mountain range. To the west and south it is bordered by the sea, and to the east the area is bordered by the beach line of the village of Almyropotamos. The N-S trending mountain range is made of massive marble. To the west and east of the mountain range, flysch and metaconglomerate units, respectively, strike approximately N-S trending. Measured foliations representing S1 dip towards NW-W. This S1 foliation is related to M1. A few measurements show that the foliation is locally dipping towards S. Foliation S1 was well discernible and could be measured well, especially in the marble. Stretching lineation measurements show a top-to-the W shearing direction. Fold structures could be recognized mainly in the metaflysch but also in the marble. The folds are isoclinal and tight and locally develop into kinkfolds. Crenulation lineations and fold axis measurements indicate a consistent E-W trend. The fold axis surface is moderately inclined striking NE-SW. In an outcrop (WGS 84 24.10649,38.27499) spectacular structures were found that provide information on the shear direction. In the outcrop, metaflysch with marble pebbles is embedded between the marble. The outcrop is part of the so called “Buffalo Shearzone”, which is estimated to be a ductile shearzone and was emplaced during late D1 deformation (Gerogiannis et al., 2021). Initially, it was suggested that the strain becomes stronger towards the metaflysch zones. This can be recognized by the strong mylonitization of the surrounding marbles. In the center of the metaflysch towards structurally higher

units, however, no shear deformation is evident, which can be seen in flattened marble pebbles in the flysch suggesting plane strain conditions. Shear indicators are limited to 2m in the metaflysch. Shear band boudinages with winged inclusions and pinch and swell structures show top-to-the-W directed extension. The formation of top-to-the-West SCC' fabrics could be assigned to D2. Furthermore, it can be observed in the outcrop that the whole fabric has been overprinted by S-folds. The fold axes dips towards the north while the fold axis plane points towards the NW. The marble pebbles embedded in the flysch are partly folded and extremely thinned. The folding could be related to a second stadium of the D1 compressional event. Brittle and ductile high angle normal faults cross cut all fabrics. While both top-to-the-west and top-to-the-east shear sense was observed in the west, opposite top-to-the-west shear sense was observed in the southern part. This is due to the formation of an east-vergent antiform. This is supported by the formation of SCC' foliations which also indicate a top-to-the-west shear sense. The dip of the S1 foliation and stretching lineations is consistent with the western part. As an indication of polyphase folding, type 2 refold structures (Ramsay and Huber, 1987) were found in the center of the southern area. The mushroom interference structures give evidence of N-W and E-W vergent folding, which will be discussed later in this master thesis. In the southern part of the southern area cataclastic zones, which are exploited by the formation of caves with speleothems, could be discovered, which give evidence for a D2 event. A fracture corridor in the south was analyzed by fracture network analysis and is discussed in more detail in chapter 5.3. Structures associated with D1 can be found distributed over the whole area. This includes the regionally differently oriented S1 foliation, which is macroscopically well recognizable and defined by regular or irregular layering (macroscopic compositional layering). The S1 foliation dips predominantly to the west. The stretching lineations in the east of the area dip consistently towards the west, whereas in the west on the peninsula of the area they dip shallow towards ENE and WSW, respectively, and partly also towards the north.

5.1.2. Northern and Middle Area

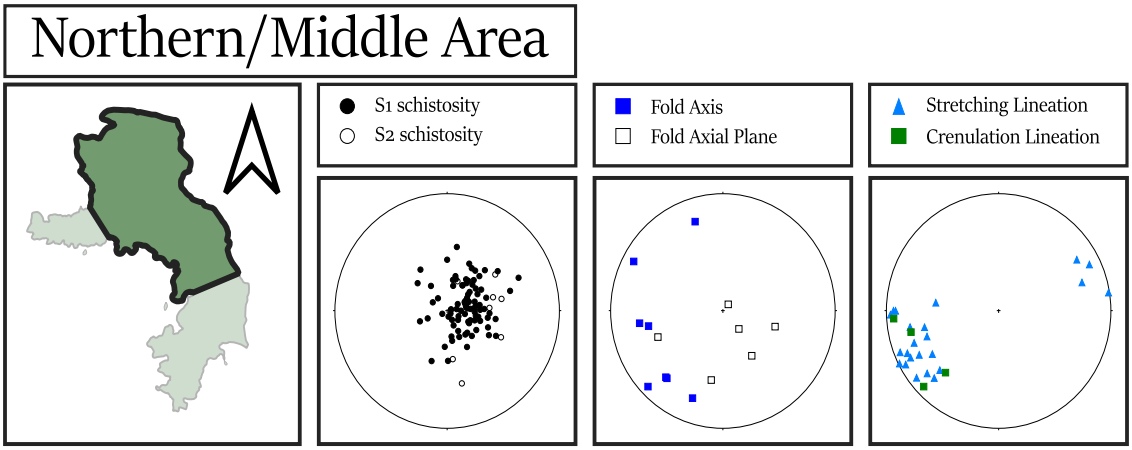

Figure 8.: The Northern and Middle area.

Measured structural data of the most important geological parameters. The Central Area gave insights in the evolution of the rocks during the subduction stage and the following extension phase during D1. Brittle Structures belonging to D2 where also found in this part. Note the mostly westwards orientation of structures. Some key outcrops gave informations about the first full ductile stage during D1.

The mountain range coming from the south continues in the central to northern part, but there is a change of direction along NW-SE. Northwest of the range, a continuation of the metaflysch units from the south could be observed, but large parts are burried below Quaternary units in the surrounding valleys of Argiro (around WGS 84 24.13610,38.31990). The S1 foliation dips predominantly westwards, with a large spread between SW and NW. Stretching lineations dip towards SW and NE. Folding is observed in the marble and metaflysch with fold axes trending between NW and SW. Fold axis surfaces constantly dip towards NW. This could be an indication of N-S-vergent folding. The folds are mostly isoclinal folds which can be attributed to D1. Pebbles in the metaflysch could be detected mainly in structurally lower units and are mostly elongated. Structures that can be used as shear sense indicators were detected in the form of pinch and swell, shear band boudinages and SCC' microstructures. The measurements show top-W directed shear, but this could not be consistently observed. The formation of a drag fold in the center of the section was spectacular. A north-south trending east-vergent synform was dragged by an approximately SW striking fault resulting in a type 2 (mushroom) refold structure. The fold axial plane that dips towards W is dragged close to the fault into a S dipping orientation. Ductile SCC' structures indicate top-to-the-S displacement of the hanging wall of a normal fault. The

folding can be assigned to D1, whereas the drag of the fold occurred later during or after D2. Joints and cracks were recognized and measured, the conjugate faults have no uniform trend but move between northwest and southeast dipping. Joints dipping to the west were also measured. These cross-cut the entire rock, which is why it can be assumed that they were formed later after M4 under brittle conditions.

5.1.3. Western Area

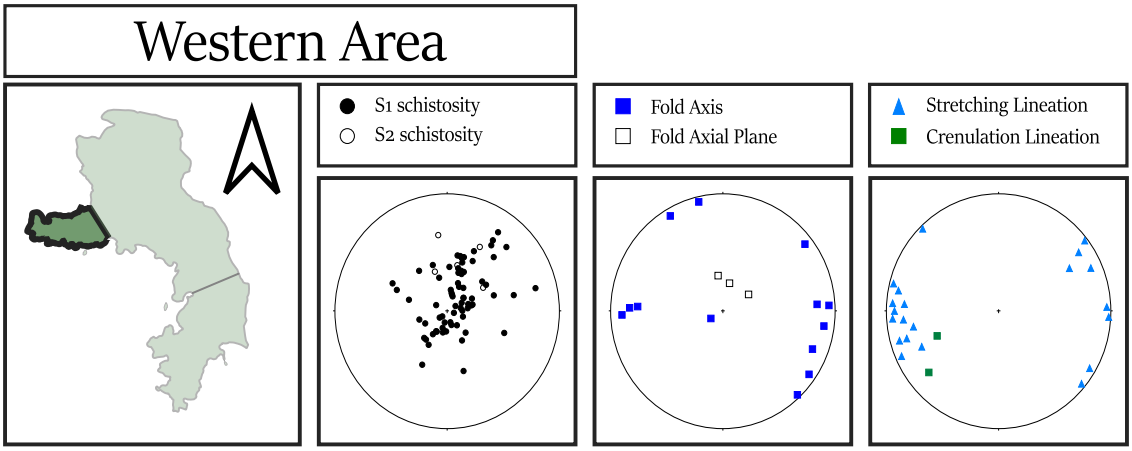

Figure 9.: The Western area.

Measured structural data of the most important geological parameters. Within the western area, all stages of deformation are recorded indicated by variations of structural data in every direction. Fold cores, which give 3D information of regional folding are found here. The area has to be further investigated due to strong deviations in structural data.

The Western part of the study area comprises a 3.5 km E-W elongated peninsula and records the most complex deformation. Although the marble units still represent the major lithology, several metaflysch layers outline the complex deformation on the peninsula. The S1 foliation records no preferred orientation and dips in all directions. Compared to the rest of the area where the assignment to deformation events was straightforward, cross cutting relationships are more difficult on the peninsula and it is likely that principle deformation directions changed during progressive deformation. Stretching lineations indicate SSW-NNE-stretching, with minor data showing NNW-SSE extension. Folding associated with D1 is observed throughout the peninsula. Fold axes dip east and westward as well as toward the NNW. Along the E-W trending, open to tight folds with straight limbs were predominantly observed, whereas isoclinal folds were more commonly observed along the N-S trending folds. The fold axial surfaces dip shallowly in either the north or south direction, supporting

a N-S directed folding. Although different high order fold geometries ranging from S, Z to M folds could be found in some areas, this information did not allow a conclusive folding model to be established. In one outcrop this is particularly remarkable as can be seen in Fig. (Show double fold). Shear sense indicators show mostly top-to-the-west but some top-to-the-east shear. Pinch and swell and shear band boudinages are predominantly found in the vicinity of metaflysch layers, also on the peninsula a mylonitization of the marbles towards metaflysch can be observed. Depending on the structural position, the marbles can vary from coarse-grained and unfoliated to very fine-grained and mylonitic. The metaflysch units vary from ultra-fine grained to coarse grained and containing marble pebbles. SCC' microstructures are consistently observed mainly in marble and show a S-SW orientation. Shear sense indicators such as boudinages and pinch and swell structures indicate a higher grade of mylonitization and can be assigned to the D1 event. A second foliation S2 which can be recognized by SCC' structures indicates a further event assigned to ductile regime. Brittle structures can be seen in the form of crosscuttings. These indicate that an E-W extension occurred first followed by a SWW-NEE extension. These extension structures indicate a post D2 deformation.

5.1.4. Results of the X-Y-Z Measurements

One of the tasks of this work was to find a tool with which it is possible to make statements about the change of strain rates. Therefore, the three principle stress axes of the strain ellipsoid were measured. In order to perform the measurements, a suitable marker was searched for, which is approximately equally distributed over the whole area. Marble pebbles in flysch zones were very suitable for this purpose. Their morphology, orientation and length distribution of the main axes allow statements about the deformation orientations of the principal finite strain axes of the strain ellipsoid. In outcrops where marble pebbles were encountered, at least 2 principal axes could be measured, but there were outcrops where marble pebbles were exposed three-dimensionally and thus all axes could be determined accurately. In general, from constrictional (cigar-shaped) to oblate (pancake-shaped) pebbles could be documented. Cigar-shaped pebbles indicate constriction and elongation, whereas pancake-shaped pebbles indicate flattening. After all data were collected, they could be plotted into a Flinn-Nadai and Hsü diagram. These are presented in the following. The results show two trends with increasing strain, one in the field of apparent constriction and one in the field of apparent flattening.

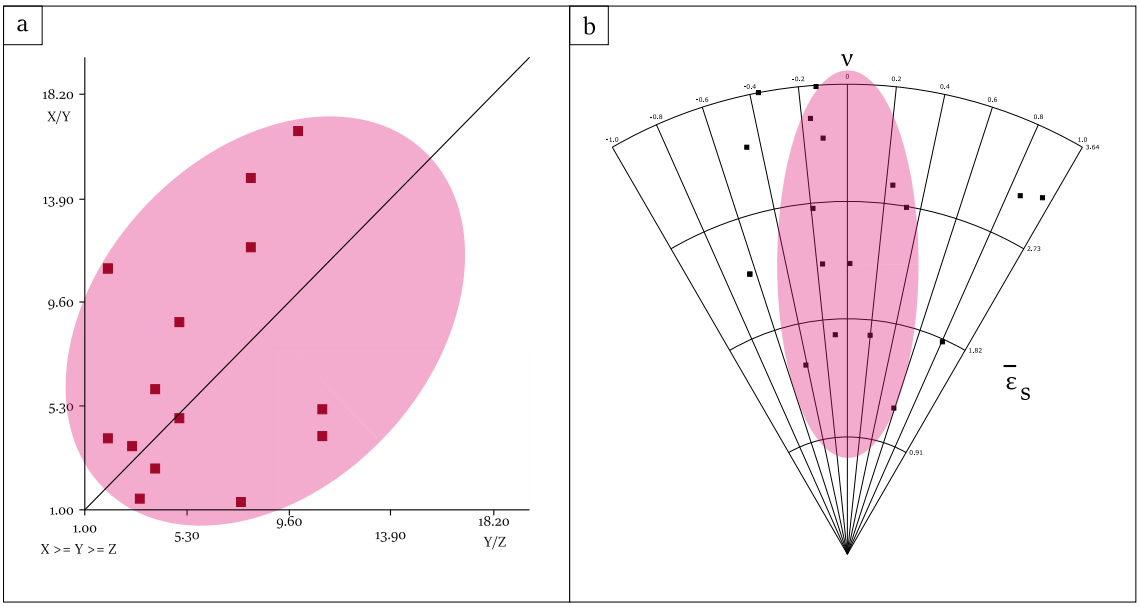

Figure 10.: Flinn- and Nadai-diagram.

(a) Flinn-diagram with all measurements of XYZ data. Y-axis defines the flattening, X-axis the thickening. Measurements are orientated along linear axis, indicating two trends with increasing strain, one in the field of apparent constriction and one in the field of apparent flattening. (b) Nadai-diagram supporting the Flinn-diagram with the conclusions.

5.1.5. Synoptikum

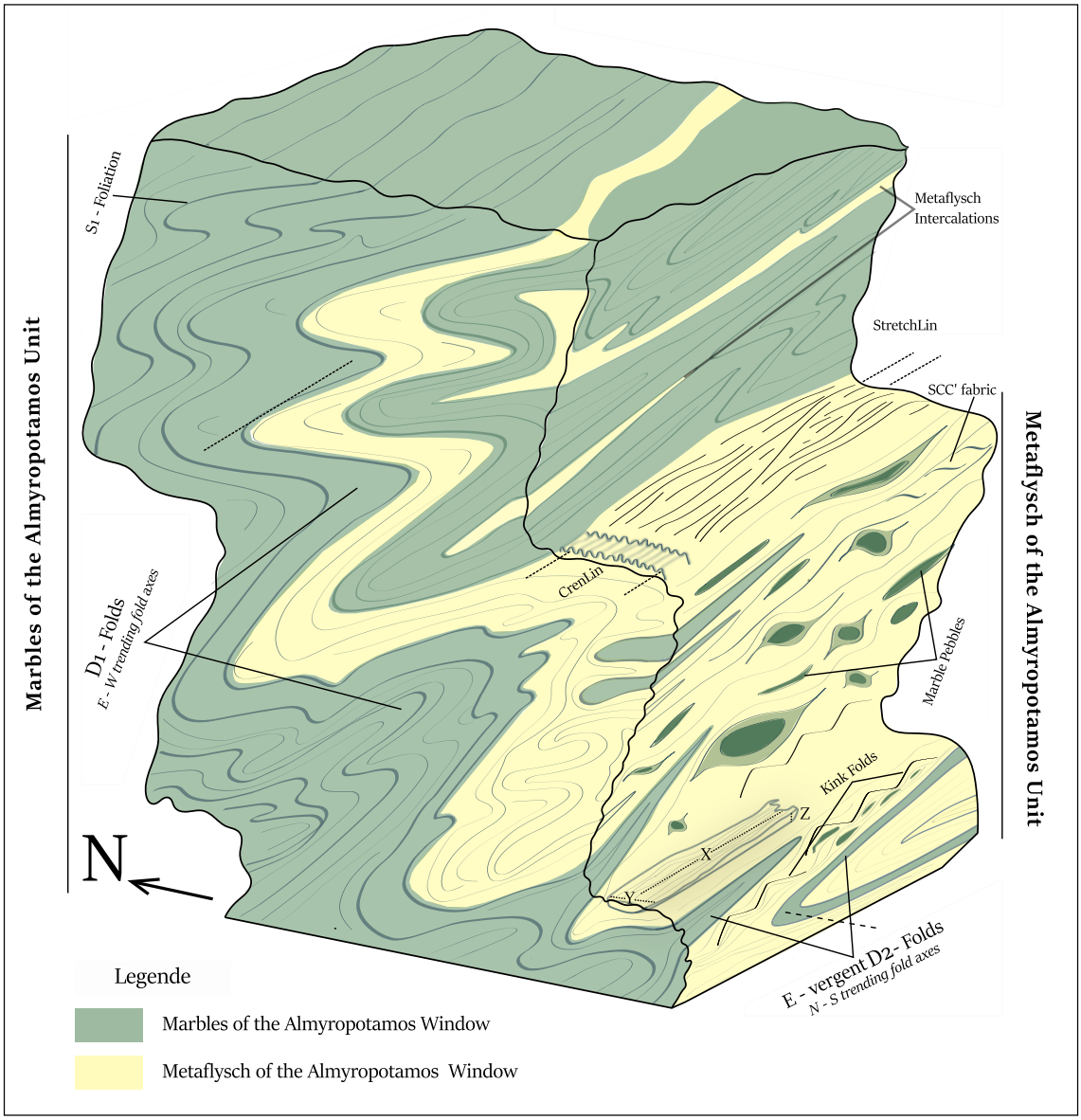

Figure 11.: Synoptical diagram

3-dimensional synoptical diagram showing all major structures detected during fieldwork.

5.2. Microstructural Analysis

During the fieldwork, a total of 29 samples were collected from different areas of the site. The samples can be divided mineralogically into 2 groups: (1) samples from the marble of the Basal Unit and Almyropotamos Unit, respectively, which have undergone different deformations and (2) samples taken from metaflysch zones.

5.2.1. Samples from the Marbles

The samples from the marble consist mainly of calcite. The calcite crystals are present in different forms, either as coarse porphyroclasts (left over grains) or as dynamically recrystallized matrix minerals and have gray, brown to white colors. Under crossed polarizers, the calcite minerals take on higher order interference colors. Calcite shows grainsize variations in some samples, from ultrafine-grained ($\sim 50\ \mu m$), mylonitic to coarse-grained (mm-range) aggregates and in some areas of diverse sections a SPO (Shape preferred orientation) can be identified. The individual grains form interlobate to polygonal crystal shapes. The main feature of the calcite crystals is the strong twinning (see Fig. 12b) which can be classified as deformation twins (Passchier and Trouw, 2005). Some marble samples show a metamorphic layered grain-dominated structure whereas others show an irregular matrix-supported structure. In some sections calcite crystals overgrow a preexisting foliation (Fig. 12e) consisting of quartz and opaque phases. Localized shear zones can be identified in some sections (Fig. 12f/h), separating coarse-grained from fine-grained areas. As secondary aggregates mainly quartz, mica minerals (biotite and muscovite) were identified, sporadically opaque minerals or heavy minerals, feldspars (albite) and chlorite can be recognized. In isolated samples flysch intercalations can be recognized, mainly consisting of detrital quartz, albite and chlorite. In samples with metamorphic layered structure shear sense indicators could be detected (Fig. 12f). Modifications of calcite like aragonite (reported in (Gerogiannis et al., 2021)) could not be found. Structures formed by lower temperatures by brittle-ductile deformation could be identified in form of SCC'-structures (Fig. 12g).

5.2.2. Samples from the Metaflysch

Samples identified as flysch show a higher diversity in mineralogy than the ones from the marbles. The mineral fabric of the metaflysch specimen shows predominantly a schistose and elongated texture or SPO (Shape preferred orientation), which means they have aligned along the main direction of shear (Fig. 12e). Porphyroclasts are surrounded by matrix minerals which consist mainly of light and dark mica (biotite, muscovite) calcites, quartzites, feldspars (albite), occasional chlorite and opaque phases. Various microstructures indicating shear sense, such as mica fish (Fig. 12d), SCC' microstructures (Fig. 12g) and calcite twinning could be detected. Furthermore, in certain sections crenulation cleavage with surrounding microlithons could be detected (Fig. 12a). The feldspars are occasionally twinned and have a poikiloblastic structure with minerals growing in the feldspar crystal. They are well recognized by their euhedral, idiomorphic structure grown over the schistosity. Mica are elongated have and serve as matrix minerals or shear zone localizers. The quartzes often occur collected in layers between shales, rather rarely as porphyroclasts, have small to large grain sizes and often show granoblastic fabrics in the form of a foam structure. Often triple grain boundaries are formed (Fig. 12c).

5.2.3. Interpretation of the Microstructures

A microstructure analysis was performed to compare the results with those of the field work and to see if there are correlations between microstructures and structures in cm - m range. Structures that allow such comparisons and were observed are:

- Deformation twinning of calcite crystals.
- Observation of crystals giving evidence of dynamic recrystallization
- Pressure solution structures
- Shear sense indicators

All samples were checked if the above mentioned structures can be found. In the majority these structures can be found and evaluated. Deformation twins are found in all samples with a few exceptions and their classification follow (Burkhard, 1993). Twinning intensity varies, but at least type I twinning could be found in nearly all samples. However, some sections contain also type II and III twinning structures, indicating elevated temperatures

(>300°C) in certain parts of the area. Support for the relative temperature indications necessary for the formation of deformation twins is provided by the width of the twins. In some sections, wide (type II) rather than thin twins are found (Fig. 12b), suggesting that with higher strain and temperature (>300°C), widening of existing deformation twins is favored rather than new formation of twins (Passchier and Trouw, 2005). In zones where it is suspected that the strain was more localized, type III twins can be found with curved, tapered and lensoid shapes. Since all forms of twins (I to III) can be found, it can be estimated that the temperatures must have been around 350°C, otherwise a complete dynamic recrystallization of calcite would occur (Passchier and Trouw, 2005).

In order to compare the results of the twin analysis, calcite or quartz crystals and their shapes were better analyzed in detail. Microstructures indicative for intracrystalline plasticity (Passchier and Trouw, 2005) suggest ductile deformation by dynamic recrystallization. These microstructures are Subgrain Rotation (SGR) and Grain Boundary Migration (GBM). SGR can be observed well at localized shear zones (Fig. 12f/h), where the grains have a small grain size, which suggests extended cooler conditions. Furthermore, the grains affected by SGR show a SPO, which is oriented along the localized shear zones (Fig. 12f). Irregular grain boundaries, lobate structures and the formation of large crystals further indicate GBM (Fig. 12h). From both mechanisms it can be deduced that strain rates decrease from GBM (higher temperatures are needed to remove dislocations and subgrain boundaries) to SGR and that temperatures increase (Passchier and Trouw, 2005). The second mechanism identified is Diffusive Mass Transfer by solution(DMT) in the form of dissolution and precipitation (Passchier and Trouw, 2005). The microstructures formed by DMT are SCC' fabric, spaced cleavage or crenulation cleavage. SCC' microstructures show a consistent W-directed sense of shear (Fig. 12g) Shear sense indicators formed by DMT were found in the flysch samples. Especially mica minerals (biotite and muscovite) which take sigmoidal forms in a SCC' structure were used to determine the shear sense (Fig. 12d). The shear sense varied from sample to sample and no trend could be detected. Quartz as a fixed component of the samples served differently in the microstructural anlysis. Thus, based on the formation of triple grain boundaries, static recrystallization or recovery of the mineral structure could be detected (Passchier and Trouw, 2005). By Grain Boundary Area Reduction (GBAR) the quartz grains tend to grow and form more and more idiomorphic

boundaries (Fig. 12c). Quartz grains show undulose extinction in all samples, indicating a persistent temperature influence on the rock structure while deformation had no further influence on the rock. Furthermore, microlithons are formed in the quartz structure, this is due to isoclinal folding (Fig. 12a). This deformation can also be found in the neighboring mica.

If the results of the microstructure analysis are compared with those of the field observations, they are generally in agreement: Coarse and large calcite crystals are relics of the M1 metamorphism. The temperatures and pressures of the blueschist facies metamorphism were sufficient to drive dynamic recrystallization of the calcite grains by grain boundary migration, which were later during exhumation overprinted by deformation twinning. Feldspar porphyroclasts do not show dynamic recrystallization constraining the M1 temperatures to <450°C. The quartz crystals with their formed triple points indicate that temperature outlasted deformation during the M1 event. Overall, temperatures of about T: <400°C can be assumed, fitting with reports which have done research for P-T conditions ((Shaked et al., 2000). Structurally, isoclinal folds with fold axis parallel to the stretching lineation can be associated with early M1 metamorphism. Very fine-grained layers in the samples or fine-grained shear zones provide evidence for greenschist facies M2 metamorphism (T: < 400°C / P: 4 - 7 kbar) (Reinecke, 1986; Lensky et al., 1997; Shaked et al., 2000).

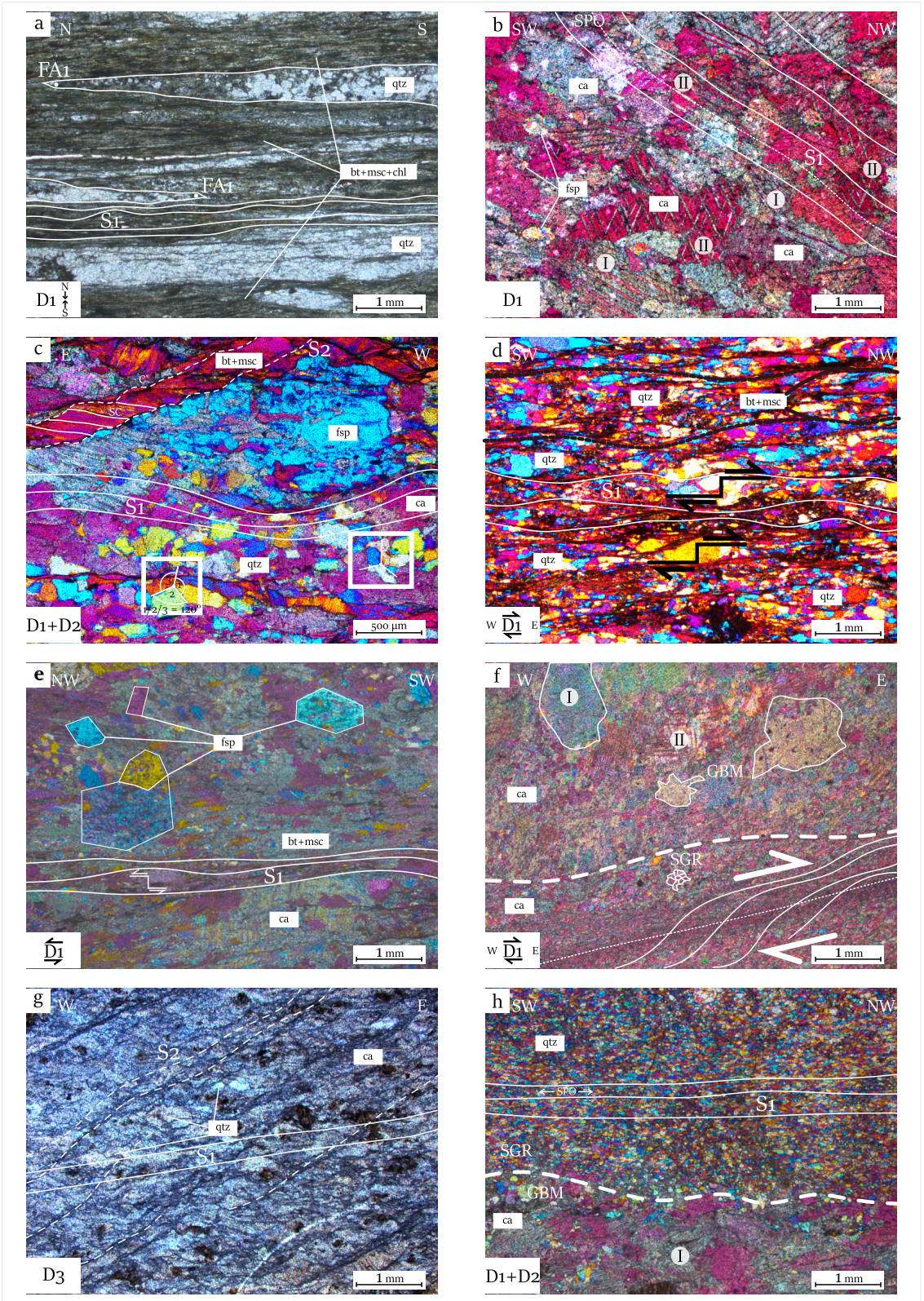

Figure 12.: Pictures of Microstructures.

(a) Microlithons in Metaflysch as indicators of D1 (UTM35 247659/4248515). (b) Dynamically recrystallized marble with twinning of calcite grains (UTM35 248563/4238869). (c) Marble with well developed grains show S1 and S2 foliations. Triple junctions of quartz grains indicate static equilibrium under high pressure (UTM35 247145/4248899). (d) Quartz grains give informations about Top-to-the-W shear sense (UTM35 247338/4248421). (e) Sharp grain boundaries of feldspar indicate max. temperatures around 400°C (UTM35 247659/4248515). (f) GBM and SGR as two main mechanisms during ductile deformation. Both areas are seperated by a shearzone (UTM35 247063/4238520). (g) Metaflysch with SCC' structures developed during D3 indicating lower P/T-conditions in contrast to D1/D2 (UTM35 241375/4246788). (h) two zones indicate strain partitioning during D1 and D2 (UTM35 240981/4246002).

5.3. Fracture Network Analysis

A Fracture Network Analysis has been carried out for a chosen area in the south of the Almyropotamos Window. The area covers 0.87 km^2 and is located in the southern part of the research area on a peninsula. The fractures could be recognized as brittle faults in the field but they are more clearly seen in the satellite images, where their intersection with the surface is decorated by the vegatation (see Figure 13). The mapped fracture pattern was further investigated by the toolbox.

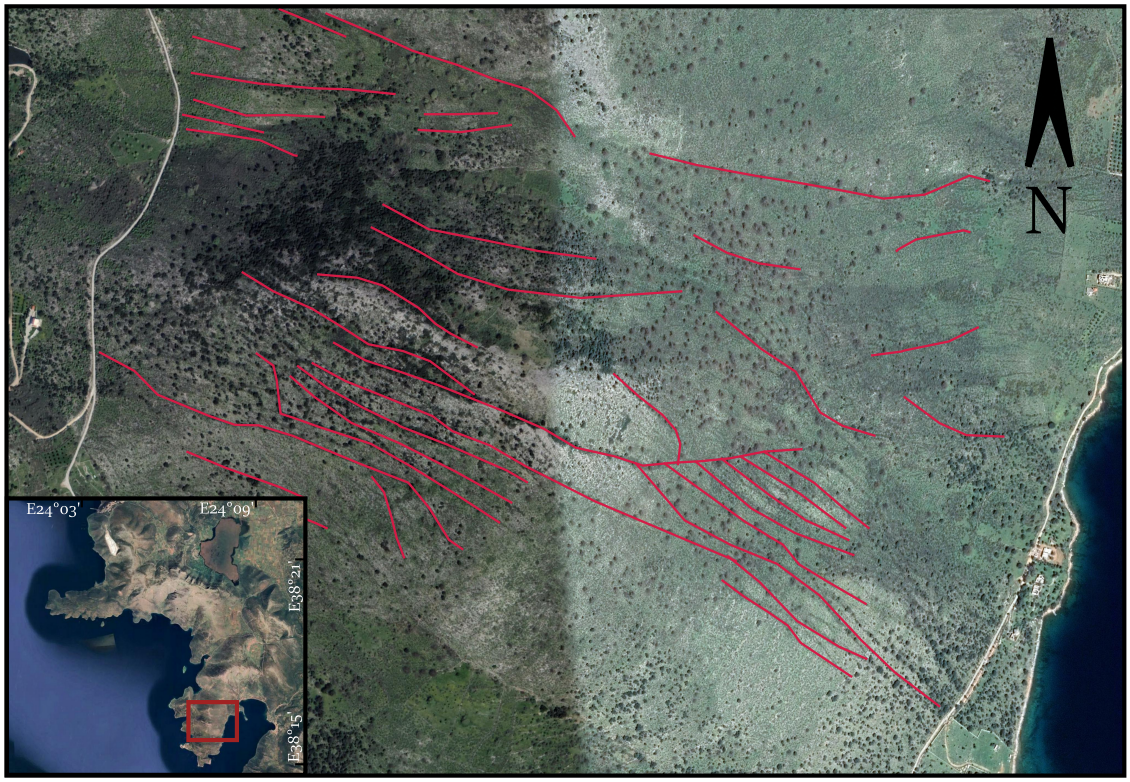

Figure 13.: Traces of the mapped fracture pattern in the Google Earth satellite image east of Almyropotamos.

Figure 14 shows the digitized fractures. The fractures are discretized in nodes, which are shown with black circles, and the individual segments, whose centers are shown with red squares. A series of segments results in a trace. The center of a full trace is shown with a red circle. The first step in FracPaQ is to identify the way the fractures are connected to each other. For this purpose the nodes are analyzed for overlaps and the results presented in Fig. 15 show that the main part of the fractures are isolated (I). However, in the southeast of the fracture corridor there some minor numbers of X and Y overlaps. X nodes indicate an

overlap of two fractures whereas a Y node represents a triple point between two fractures.

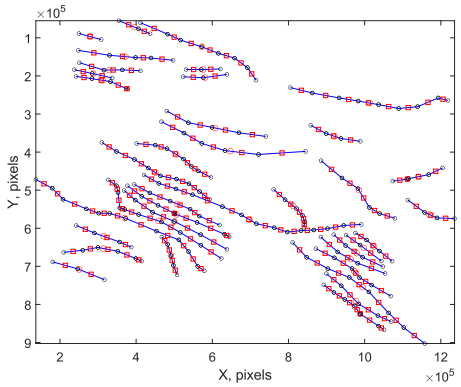

Figure 14.: Mapped traces (n=37), segments (n=176) and nodes (n=213).

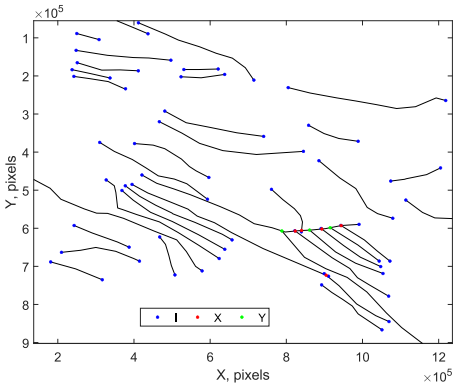

Figure 15.: Connectivity node types n(I)=67, n(Y)=3, n(X)=5.

Since the program has recognized the fractures in the form of traces and segments, the lengths, frequency distribution of lengths and orientations of each fracture can be calculated. Figure 16 shows that the segments most frequently have a length of about 90 meters. Traces (Fig. 17 as a composite of segments often have lengths in the range of 270 to 700 meters. As can be seen in Figure 18, fractures mainly strike along WSW - ENE.

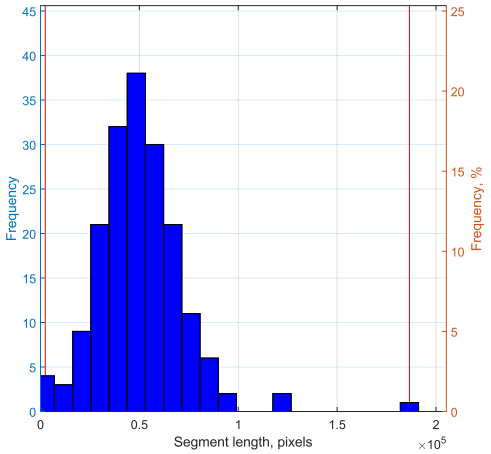

Figure 16.: Length distribution of segments.

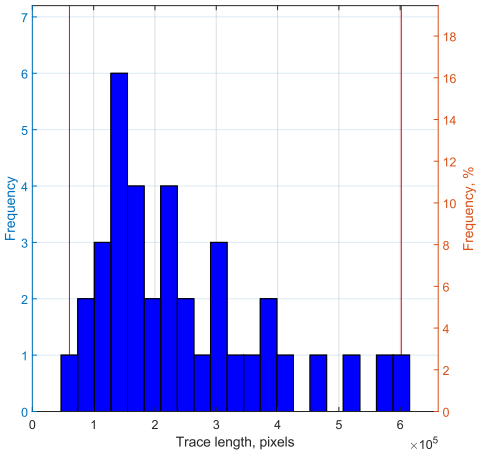

Figure 17.: Length distribution of traces.

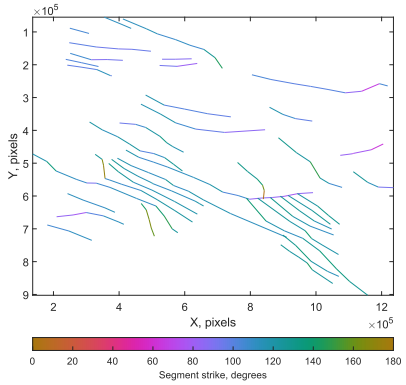

Figure 18.: Orientation of Fractures

With FracPaQ it is also possible to perform more complex calculations like quantifying the slip tendency of discontinuities in a given stress field (Morris et al., 1996). The main factor for the possibility of slipping of a surface is the ratio between normal and shear. If the ratio between normal stress (σ) and shear stress (τ) is greater than 1, it is very likely that the area will slide. To calculate the slip tendency, FracPaQ takes default values for sigma. Fractures striking along NW-SE tend to slip more than fractures striking E-W or N-S, as can be seen in Figures 19 and 20.

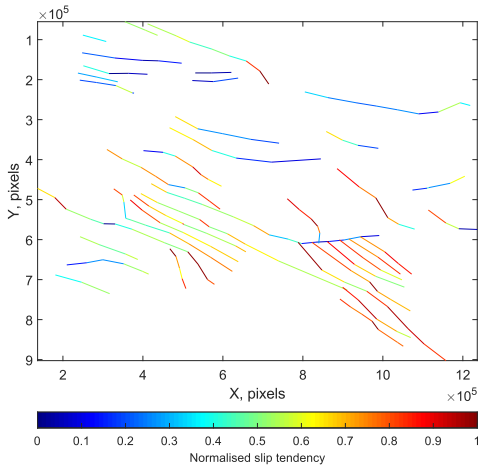

Figure 19.: Slip tendency for digitized traces, segments and nodes.

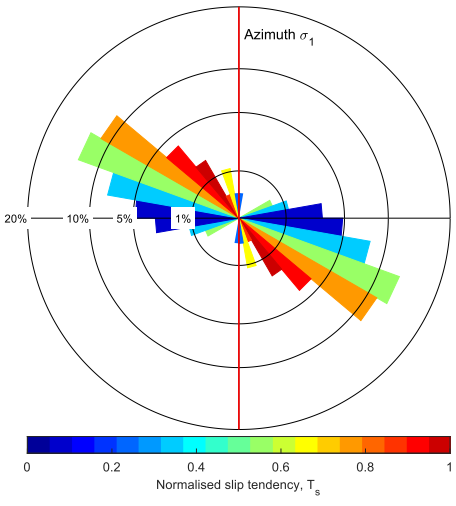

Figure 20.: Slip tendency presented in a equal area rose plot.

Another important point of analysis is the evaluation of the X-Y-I connectivity to make statements about connected fluid flow. The calculated blue point in Figure 21 shows that the fracture network tends to isolated fractures and not to connected ones, otherwise the point would be rather in the lower range.

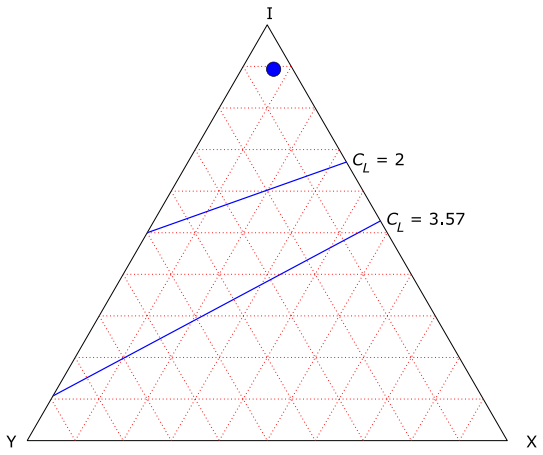

Figure 21.: X-Y-Z-Connectivity

Based on the parallel plate model of fractures (Oda et al., 1987), permeability calculations (Fig. 22 can be calculated for the area. For this purpose, default parameters are included in the calculation algorithm to create a permeability plot. Similar to the slip tendency, fractures that strike WNW-ESE tend to have a higher permeability than fractures that are oriented differently. In a crack tensor plot (Fig. 23, orientation data are combined with length data and spatial density of fractures. The result is a dimensionless crack pattern whose different orders can be assigned to other physical properties such as permeability (2nd), elasticity, or acoustic velocity. Since the calculation of the crack tensor is based on the poles of the fracture trace segments, the tensors are perpendicular to the calculations from permeability and slip tendency along NW-SE.

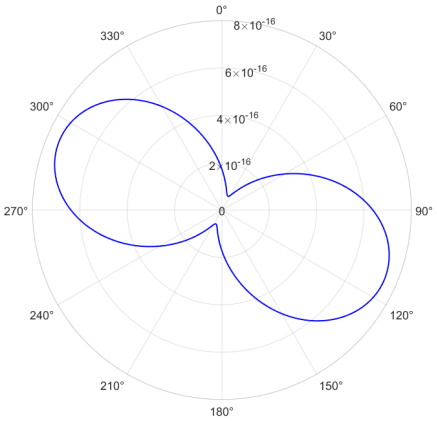

Figure 22.: Permeability Plot

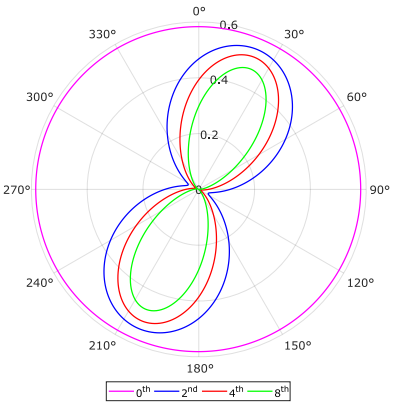

Figure 23.: Crack Tensor Plot

Finally, a calculation was made if the fractures in the area tend to fail. For given parameters, a Mohr stress diagram (Fig. 24) was generated from which the tendency of the fractures not to fail can be deduced.

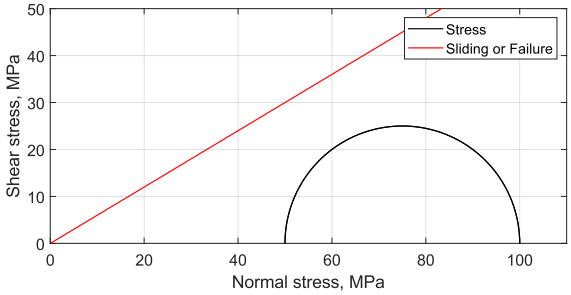

Figure 24.: Mohr stress diagramm

6. The Polyphase Evolution of the Almyropotamos Window

In the following chapter the polyphase evolution of the Almyropotamos Window is discussed. Based on field observation and microstructural analysis a consistent model of the evolution is presented. It should be noted that the classification of events like Deformation Events (D) rely on the results of the fieldwork and are meant to describe relationships between all types of structures and time.

6.1. Early Stage and beginning of subduction at the end of the Eocene

The subduction of the Cycladic Blueschist Units (CBU), which started during the Late Cretaceous, did not affect the units of the Almyropotamos Unit on Evia (Shaked et al., 2000). Fossil finds on top of the marble units of the AU indicate that sedimentation must have occurred in a carbonate platform setting until at least the middle Eocene (Dubois and Bignot, 1979). While the marble unit of the AU was already affected by subduction, sedimentation of the protoliths of metapelites or metaconglomerates continued until at least the end of the Eocene/beginning of the Oligocene (Dubois and Bignot, 1979; Katsikatsos et al., 1986). Compressional forces triggered by subduction of the African plate, already acting since the end of the Cretaceous in what is now the Aegean, led to thrusting of the allochthonous CBU over the paraautochthonous AU at the beginning of the Oligocene, initiating high-pressure metamorphism and thus the onset of D1 (Xypolias et al., 2003). D1 represents a ductile deformational event that structurally affect both the AU and the units of the CBU. The D1 metamorphism occurred under blueschist-conditions (400°C

/ 8-10 kbar) and resulted in the formation of an S1 foliation (Dürr et al., 1978; Avigad et al., 1997) and large-region folding (Shaked et al., 2000) during subduction. The region was characterized by flattening due to strong compressional forces through burial and the creation of ductile shearzones like the Buffalo-Shearzone (see Figure 4) in the west of the study area . This can be evidenced by extremely oblate pebbles (Fig. 3f) and strongly mylonitisized dolomite layers in metaflysch units (Fig. 3b) which indicate very high shear-strains. S1 shows mainly north-southwards dipping and underthrusting of the CBU by the AU results in shear processes and thinning of the S1 foliation, which is subsequently folded with N-S striking fold axes. The fold axial planes are subparallel to the main S1 foliation, the fold axes subparallel to measured stretching lineations. The newly formed folds can be seen in the form of isoclinal folds and form thinned legs and thickened fold hinges. While previous works (Gautier and Brun, 1994; Xypolias et al., 2003) argue for SE-directed thrusting based on stretching lineations, the results of this work and other studys (Shaked et al., 2000) argue for an earlier ductile folding event that is E-W directed. Crenulation lineations analyzed in samples of metaflysch from the western part of the area support a first folding event belonging to D1. N and S dipping axial plane schistosity support the hypothesis of in the early stage of subduction.

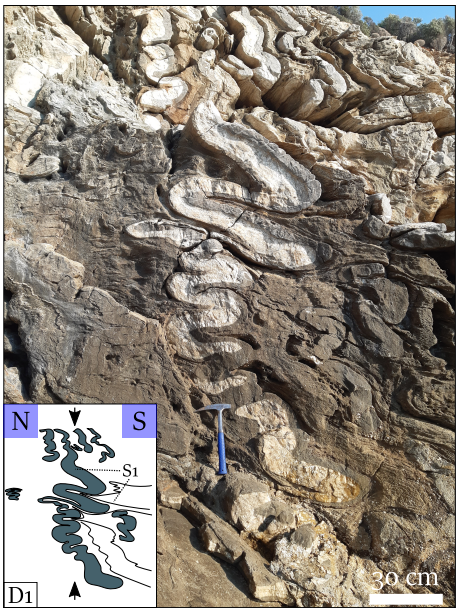

Figure 25.: Fold-core zone.

Fold-core Zone with flattened dolomite layers in the metaflysch-units of the AU. Subduction during M1 is resulting in flattening and subsequent folding of all units in the Almyropotamos Window along N-S (UTM35 239972/4246849).

6.2. Beginning of Exhumation and Main Metamorphism during Oligocene

In a second stage during the end of the Miocene where the peak of the high-pressure metamorphism was reached, an E-vergent folding occurs. This folding event is equivalent with the second stage of the evolution of the Almyropotamos Window and is declared as D2 stage. D2 has been described in previous researches (Xypolias et al., 2003; Ring et al., 2007) but in contrast to this work it is described as the first folding event, which is in contradiction with D1. The second folding event belonging to D2 crosses the whole area and leads to a reorientation of the S1 foliation which now dips mainly towards the west and to the formation of fold axes which are mainly directed N-S to NW. Folds assigned to D2 can be seen predominantly in the eastern part of the area, thinned and doubled flysch zones between the marbles show consistent west-trending stretching lineations. Folding related to D2 resulted in further formation of an axial plane foliation that also dips consistently at an average of 30 degrees toward the west. The E- vergent fold structure, which is shown in the profiles (Figures 5 and 6), belongs to the main deformational events during ductile evolution of the Almyropotamos Window. Markers supporting the E-vergent folding of the study area are marble pebbles in the metaflysch that are elongated and adjusted along the main E-W foliation, as well as stretching lineations that are west-directed. One type-2 Mushroom structure found in the southern area (see Fig. 3c) and an outcrop in the western area showed folding of higher order striking N-S and E-W (Fig. 26b+c), which would be consistent with two folding events during D1 and D2. Microstructural analysis supports D2 as the main deformation event. Calcite crystals show strong dynamic recrystallization consistent with the conditions of blueschistfacies metamorphism. SGR and GBM as main mechanisms support data from previous research indicating similar pressure/temperature conditions like D1 (8-10 kbar/ 400°C). Deformation twins serve as another indicator, especially the formation of type II to III twins shows that widening of twins at temperatures above 200 degrees are favored than formation of new ones (Passchier and Trouw, 2005). Since feldspar was not dynamically recrystallized, a temperature maximum of about 400 degrees can also be given above, which is consistent with previous works (Shaked et al., 2000). Quartz grains, which particularly often have straight grain boundaries with triple junctions, suggest

that static recrystallization occured under elevated temperatures but without significant differential stress. D2 is already associated with the end of subduction and beginning of the exhumation of the AU.

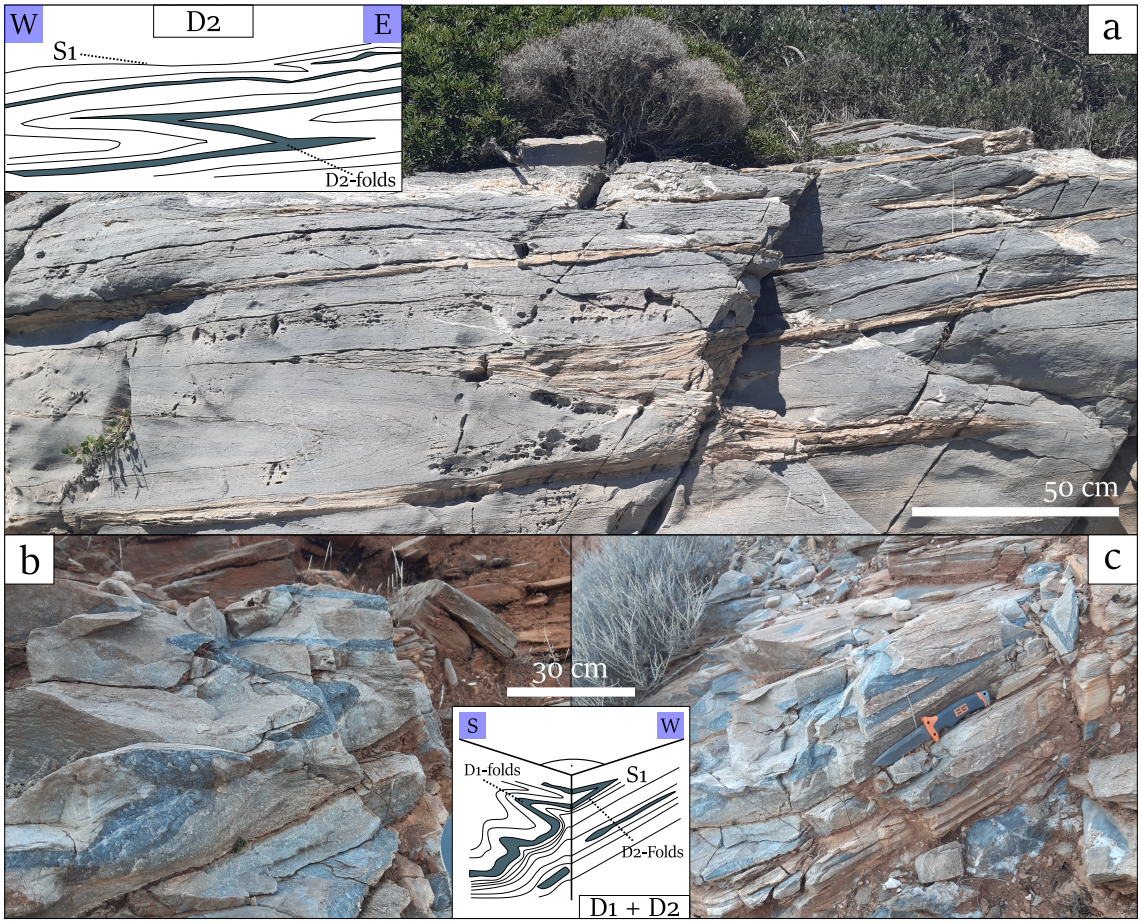

Figure 26.: Pictures of structures belonging to D1 and D2.

(a) E-vergent Folds as a result of D2 during exhumation of the AU (UTM35 240415/4246036). (b+c) showing 3D-outcrop with two different fold generations perpendicular to each other. (b) shows typical wavy ductile forms (D1), whereas (c) tends to sharp planes due to lower P/T-conditions during D2 (UTM35 242323/4245908).

6.3. Reactivation of the Buffalo Shear Zone during exhumation

The reactivation of ductile fault zones in the west of the area is attributed to a metamorphism belonging to deformational event D3. These reactivated fault zones, for example the Buffalo Shear Zone, represent the end of the ductile to brittle-ductile deformation phases (D1-D3) and are responsible for an E-W directed extension of the area. Previously, the Buffalo Shearzone was described as a N-S striking section in the western part of the area (Gerogiannis et al., 2021). However, there is strong evidence that this does not stop in previously mentioned section, but continues northward before making a turn toward W-NW at about halfway up the area (see Figure 4). Strong mylonitization is evident in the surrounding marbles. Boudinages and pinch and swell structures suggest an E-W extensional regime. Shear-sense indicators with top-to-the-west shear sense were recognized in samples from the Buffalo Shear Zone. A drag zone (see sketch in Figure 5) in the central part of the area supports a brittle-ductile deformation event, where a fold core folded by D2-folding was refolded by dragging into the reactivated Buffalo shearzone. Slickenfibres further indicate that dissolution-precipitation has been a main mechanism during D3. The temperature and pressure conditions have been lower than during D3 and is related to a greenschist facies metamorphism (320 $\pm$ 40/ 7 $\pm$ 1 kbar) that affected the entire area. Rb-Sr measurements yield values indicative of D3 prior to 23 Ma (Bröcker et al., 2004). Recent work supports the estimated metamorphic conditions and ages ((Ducharme et al., 2022). By the results of this study, it is estimated that the reactivation of the Buffalo Shearzone can be related to the formation of the NCDS. The NCDS formed in the Oligocene and is responsible for the onset of extensional processes in the Aegean and subsequently for the exhumation of various magmatically formed domes and, in this case, for the final exhumation of the deeply subducted blueschist units and units of the AU (Jolivet and Brun, 2010). Activation of old fault zones by the NCDS led to decompression of units on Evia and thus to temperature and pressure decreases toward the end of the Oligocene (Katzir et al., 2000; Jolivet and Brun, 2010). This is contemporaneous to the end of D3. By looking at the morphology of the area in comparison to the pathway of the NCDS, which also strikes along N-S, it seems that the Buffalo Shearzone has similar N-S orientation like the NCDS,

but this must be further investigated.

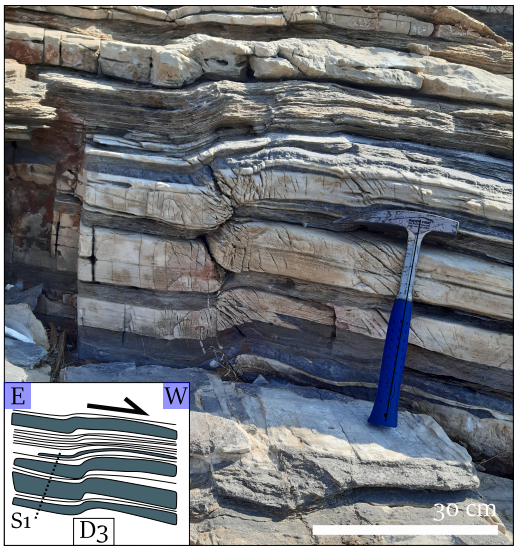

Figure 27.: Dolomitic marble layer.

Outcrop showing mylonitisized layers of marble and dolomite. Stretching lineations on top of dolomite indicate westward-extension during D3. (UTM35 240042/4247297).

6.4. Syn-orogenic Extension and Exhumation

The final stage of the evolution of the Almyropotamos tectonic window is related to a new deformation event D4. D4 is the onset of the latest and coldest deformation phase, in which the tectonic window of Almyropotamos has been completely exhumated. The metamorphic conditions during D4 are assigned to the brittle regime. The exhumation of the low-lying units of Evia (CBU and AU), which already started in the Oligocene, continues in the Miocene, but the localized temperatures and pressures (300°C / 4- 6 kbar) are lower than at the end of D3 (Reinecke, 1986; Lensky et al., 1997; Katzir et al., 2000), so the deformation in this time interval can no longer be assigned to the greenschist facies but rather to the pumpellyte facies. In the area this is confirmed by clay gouges in cataclastic zones. Measurements in these cataclastic zones reveal top-to-the-E directed backthrusting. SCC' microstructures (Fig. 12g) support the orientation of the backthrusting. The cataclasites are predominantly manifested in the metaflysch (Fig. 3e), samples show extremely small grain sizes thus ruling out dynamic recrystallization and confirming cooler temperatures as previously described. The exact ages of this M4 stage during D2 is the topic of further discussions.

7. Conclusion

Geological Mapping by remote sensing and fieldwork, structural and analytical investigations have been carried out near the village Almyropotamos on the island of Evia, Greece. Main focus was a tectonic window, called the Almyropotamos Window, where rocks of the Cycladic Basement Unit, locally called Almyropotamos unit, crop out. In this work, new structural data and a new geological map with two profiles are presented. Furthermore, a microstructural analysis has been carried out to understand better the mechanisms affecting the polyphase deformation of the Almyroptomas Window. As an additive, a fracture network analysis has been carried out via FracPaq in a fracture corridor in the south of the study area. From the results of this study, following conclusions can be made:

1. By detailed fieldwork it can be concluded that the metaflysch layers were deposited as a single wildflysch unit on top of the marbles and were subsequently folded within the marbles.

2. The results of the strain analysis suggest that the deformation in the Almyropotamos Window was mainly localized in the fold limbs of the metaflysch.

3. The Almyropotamos Window is the result of different folding and shearing stages during subduction (D1) and exhumation (D2 - D4) of the marble and flysch units.

4. The different stages of subduction and exhumation are documented in different areas throughout the study area.
4.1. Subduction (D1) of the flysch and marbles units is suggested to take place at the end of the Eocene/beginning of the Oligocene (30 Ma) under blueschist-conditions (8-10 kbar/400°C) (Shaked et al., 2000).

4.2. A first folding event connected with the subduction of the local units (Almyropotamos Unit) took place under flattening conditions by isoclinal folding with fold axes parallel to E-W trending stretching lineations during the Oligocene.
4.3. A second folding event (D2) lead to an east-vergent folding of the AU accompanied by Top-to-the-East shearing and exhumation of the units in the end of the Oligocene/beginning of the Miocene indicating D2-metamorphism.
4.4. A ductile shearzone, called the Buffalo Shearzone, has been reactivated during D3, which lead to an extension along E-W below the Northern Cycladic Detachment System (NCDS) under greenschist conditions (4-7kbar/350°C) according to Rb-Sr phengite-ages (Bröcker et al., 2004).
4.5. The whole study area underwent Top-to-the-East backthrusting (D4) along brittle cataclastic shearzones in the late Miocene. Temperatures did not reach 300°C.

5. The main deformation mechanism which could be detected in several specimen were intracrystalline plasticity, showing subgrain rotation and grain boundary migration as main microstructures and diffusive mass transfer by solution, showing dissolution and precipitation. Quartz grains show static recrystallization or recovery in form of grain boundary area reduction (GBAR).

6. XYZ-measurements of the principle axes of marble pebbles in the flysch layers show two trends with increasing strain, one in the field of apparent constriction and one in the field of apparent flattening.

7. The Fracture Network Analysis shows different, non-representative results, by which can be concluded, that the fractures in the area do not tend to further failure.

Bibliography

Aravadinou, E. and Xypolias, P. (2017). Evolution of a passive crustal-scale detachment (syros, aegean region): Insights from structural and petrofabric analyses in the hanging-wall. *Journal of Structural Geology*, 103:57–74.

Avigad, D., Garfunkel, Z., Jolivet, L., and Azañón, J. M. (1997). Back arc extension and denudation of mediterranean eclogites. *Tectonics*, 16(6):924–941.

Bröcker, M., Bieling, D., Hacker, B., and Gans, P. (2004). High-si phengite records the time of greenschist facies overprinting: implications for models suggesting mega-detachments in the aegean sea. *Journal of Metamorphic Geology*, 22(5):427–442.

Burkhard, M. (1993). Calcite twins, their geometry, appearance and significance as stress-strain markers and indicators of tectonic regime: a review. *Journal of Structural Geology*, 15(3-5):351–368.

Burov, E., Francois, T., Yamato, P., and Wolf, S. (2014). Mechanisms of continental subduction and exhumation of hp and uhp rocks. *Gondwana Research*, 25(2):464–493.

Dubois, R. and Bignot, G. (1979). Presence d'un "hard ground" nummulitique au de la serie cretacee d'almyropotamos (eubee meridionale, grece). *Academie des Sciences Comptes Rendus*, 289:993–995.

Ducharme, T., Schneider, D., Grasemann, B., Klonowska, I., and Soukis, K. (2022). *Exhumation of Eocene high-pressure metamorphic rock by coaxial flattening below a Miocene Cycladic-style detachment.*

Dürr, S., Altherr, R., Keller, J., Okrusch, M., and Seidel, E. (1978). The median aegean crystalline belt: stratigraphy, structure, metamorphism, magmatism. *Alps, Apennines, Hellenides. Inter-Union Commission*, 38:455–476.

Fytikas, M., Innocenti, F., Manetti, P., Peccerillo, A., Mazzuoli, R., and Villari, L. (1984). Tertiary to quaternary evolution of volcanism in the aegean region. *Geological Society, London, Special Publications*, 17(1):687–699.

Gautier, P. and Brun, J.-P. (1994). Ductile crust exhumation and extensional detachments in the central aegean (cyclades and evvia islands). *Geodinamica Acta*, 7(2):57–85.

Gerogiannis, N., Aravadinou, E., Chatzaras, V., and Xypolias, P. (2021). Calcite pseudomorphs after aragonite: A tool to unravel the structural history of high-pressure marbles (evia island, greece). *Journal of Structural Geology*, 148:104373.

Gerogiannis, N. and Xypolias, P. (2017). Retroward extrusion of high-pressure rocks: An example from the hellenides (pelion blueschist nappe, nw aegean). *Terra Nova*, 29(6):372–381.

Gessner, K., Ring, U., Passchier, C. W., and Güngör, T. (2001). How to resist subduction: evidence for large-scale out-of-sequence thrusting during eocene collision in western turkey. *Journal of the Geological Society*, 158(5):769–784.

Goscombe, B. D., Passchier, C. W., and Hand, M. (2004). Boudinage classification: end-member boudin types and modified boudin structures. *Journal of structural Geology*, 26(4):739–763.

Grasemann, B., Huet, B., Schneider, D. A., Rice, A. H. N., Lemonnier, N., and Tschegg, C. (2018). Miocene postorogenic extension of the eocene synorogenic imbricated hellenic subduction channel: New constraints from milos (cyclades, greece). *GSA Bulletin*, 130(1-2):238–262.

Haubold, H., Scholger, R., Kondopoulou, D., and Mauritsch, H. J. (1997). New paleomagnetic results from the aegean extensional province. *Geologie en Mijnbouw (Geology and Mining)*, 76(1/2):45–55.

Healy, D., Rizzo, R. E., Cornwell, D. G., Farrell, N. J., Watkins, H., Timms, N. E., Gomez-Rivas, E., and Smith, M. (2017). Fracpaq: A matlab™ toolbox for the quantification of fracture patterns. *Journal of Structural Geology*, 95:1–16.

Jackson, J. (1994). Active tectonics of the aegean region. *Annual Review of Earth and Planetary Sciences*, 22(1):239–271.

Janković, S. (1997). The carpatho-balkanides and adjacent area: a sector of the tethyan eurasian metallogenic belt. *Mineralium Deposita*, 32(5):426–433.

Jolivet, L. (2001). A comparison of geodetic and finite strain pattern in the aegean, geodynamic implications. *Earth and Planetary Science Letters*, 187(1-2):95–104.

Jolivet, L. (2003). Subduction tectonics and exhumation of high-pressure metamorphic rocks in the mediterranean orogens. *American Journal of Science*, 303(5):353–409.

Jolivet, L. and Brun, J.-P. (2010). Cenozoic geodynamic evolution of the aegean. *International Journal of Earth Sciences*, 99(1):109–138.

Jolivet, L., Daniel, J. M., Truffert, C., and Goffé, B. (1994). Exhumation of deep crustal metamorphic rocks and crustal extension in arc and back-arc regions. *Lithos*, 33(1-3):3–30.

Jolivet, L., Lecomte, E., Huet, B., Denèle, Y., Lacombe, O., Labrousse, L., Le Pourhiet, L., and Mehl, C. (2010). The north cycladic detachment system. *Earth and Planetary Science Letters*, 289(1-2):87–104.

Katsikatsos, G., Migiros, G., Triantaphyllis, M., and Mettos, A. (1986). Geological structure of internal hellenides (e. thessaly-sw macedonia. euboea-attica-northern cyclades islands and lesvos). *IGME*, (Geol. and Geoph. Res., Special Issue):191–21.

Katzir, Y., Avigad, D., Matthews, A., Garfunkel, Z., and Evans, B. W. (2000). Origin, hp/lt metamorphism and cooling of ophiolitic mélanges in southern evia (nw cyclades), greece. *Journal of Metamorphic Geology*, 18(6):699–718.

Kissel, C., Speranza, F., and Milicevic, V. (1995). Paleomagnetism of external southern and central dinarides and northern albanides: Implications for the cenozoic activity of the scutari-pec transverse zone. *Journal of Geophysical Research: Solid Earth*, 100(B8):14999–15007.

Lensky, N., Avigad, D., Garfunkel, Z., and Evans, B. W. (1997). The tectono-metamorphic

evolution of blueschists in south evia, hellenide orogenic belt (greece). *Israel Geological Society Annual Meeting*, pages 66–67.

Martha, S. O., Dörr, W., Gerdes, A., Petschick, R., Schastok, J., Xypolias, P., and Zulauf, G. (2016). New structural and u–pb zircon data from anafi crystalline basement (cyclades, greece): constraints on the evolution of a late cretaceous magmatic arc in the internal hellenides. *International Journal of Earth Sciences*, 105(7):2031–2060.

Morris, A., Ferrill, D. A., and Brent Henderson, D. (1996). Slip-tendency analysis and fault reactivation. *Geology*, 24(3):275.

Oda, M., Hatsuyama, Y., and Ohnishi, Y. (1987). Numerical experiments on permeability tensor and its application to jointed granite at stripa mine, sweden. *Journal of Geophysical Research: Solid Earth*, 92(B8):8037.

Okrusch, M. and Bröcker, M. (1990). Eclogites associated with high-grade blueschists in the cyclades archipelago, greece: A review. *European Journal of Mineralogy*, 2(4):451–478.

Passchier, C. W. and Trouw, R. A. J. (2005). *Microtectonics*. Springer, Berlin [u.a.], 2., rev. and enlarged ed. edition.

Pe-Piper, G. and Piper, D. J. (2006). Unique features of the cenozoic igneous rocks of greece. In Dilek, Y. and Pavlides, S., editors, *Postcollisional Tectonics and Magmatism in the Mediterranean Region and Asia*. Geological Society of America.

Pe-Piper, G. and Piper, D. J. (2007). Neogene backarc volcanism of the aegean: New insights into the relationship between magmatism and tectonics. In Beccaluva, L., Bianchini, G., and Wilson, M., editors, *Cenozoic Volcanism in the Mediterranean Area*. Geological Society of America.

Pe-Piper, G. and Piper, D. J. W. (2002). *The igneous rocks of Greece: The anatomy of an orogen ; with 11 tables*, volume Bd. 30 of *Beiträge zur regionalen Geologie der Erde*. Borntraeger, Berlin and Stuttgart.

Ramsay, J. G. and Huber, M. I. (1983-1987). *The techniques of modern structural geology*. Academic Press, London.

Reinecke, T. (1986). Phase relationships of sursassite and other mn-silicates in highly oxidized low-grade, high-pressure metamorphic rocks from evvia and andros islands, greece. *Contributions to Mineralogy and Petrology*, 94(1):110–126.

Ring, U., Gessner, K., Güngör, T., and Passchier, C. W. (1999). The menderes massif of western turkey and the cycladic massif in the aegean—do they really correlate? *Journal of the Geological Society*, 156(1):3–6.

Ring, U., Glodny, J., Will, T., and Thomson, S. (2007). An oligocene extrusion wedge of blueschist-facies nappes on evia, aegean sea, greece: implications for the early exhumation of high-pressure rocks. *Journal of the Geological Society*, 164(3):637–652.

Ring, U., Glodny, J., Will, T., and Thomson, S. (2010). The hellenic subduction system: High-pressure metamorphism, exhumation, normal faulting, and large-scale extension. *Annual Review of Earth and Planetary Sciences*, 38(1):45–76.

Shaked, Y., Avigad, D. O., and Garfunkel, Z. V. (2000). Alpine high-pressure metamorphism at the almyropotamos window (southern evia, greece). *Geological Magazine*, 137(4):367–380.

von Quadt, A., Moritz, R., Peytcheva, I., and Heinrich, C. A. (2005). 3: Geochronology and geodynamics of late cretaceous magmatism and cu–au mineralization in the panagyurishte region of the apuseni–banat–timok–srednogorie belt, bulgaria. *Ore Geology Reviews*, 27(1-4):95–126.

Xypolias, P., Kokkalas, S., and Skourlis, K. (2003). Upward extrusion and subsequent transpression as a possible mechanism for the exhumation of hp/lt rocks in evia island (aegean sea, greece). *Journal of Geodynamics*, 35(3):303–332.

Acronyms

.svg Scaled Vector Graphics. 11

AU Almyropotamos Unit. 5

BU Basal Unit. 5

CBU Cycladic Blueschist Unit. v

DMT Diffusive Mass Transfer by solution. 31

EBU Evia Blueschist Unit. 6

FracPaQ Fracture Pattern Quantification. 11

GBAR Grain Boundary Area Reduction. 31

GBM Grain Boundary Migration. 31

NCDS Northern Cycladic Detachment System. vi, 7

SGR Subgrain Rotation. 31

SPO Shape preferred orientation. 29, 30

List of Figures

A. Appendix

A.1. Field measurements

Nummer	A1	A1	A1	A1	A1	A1	A1	A1	A1
LocNr.	**A01**	**A03**	**A04**	**A05**	**A09**	**A11**	**A12**	**A13**	**A17**
Lithology	K	K	K	K	M	M	M	M	M
PLANE	S0		S0		Vein	Vein	S0		
DIP_DIREC	124		138		140	258	288	270	
DIP	10		30		50	43	35		
LINEATION	StrLIN		StrLIN	StrLIN			StrLIN		StrLIN
DIP_DIREC	110		250	230			260		324
DIP	14		18	30			33		25
FA DIP_DIR		320							
FA DIP		33							
AP DIP-DIR		50							
AP DIP		83							
LAT_N_S	249601,14	249677,96	249680,04	249678,36	249782,19	249870,51	249920,37	249941,45	250044,67
LON_E_W	4240388,6	4241443,7	4241542,2	4241606,7	4241854,9	4241936,1	4241931,4	4241925,1	4241930,6
ALTITUDE	21	11	130	133	157	157	5	181	180
Probennr									

Nummer	A1	A1	A1	A1	A1	A1	A1	A1	A1
LocNr.	**A19**	**A20**	**A25**	**A27**	**A29**	**A30**	**A31**	**A31**	**A33**
Lithology	M	K	F	M	F	K	K	K	K
PLANE	S0	S0	S0	S0 + Fault	S0	S0	S0	S1	S0
DIP_DIREC	328	312	301	261	291	258	294	297	300
DIP	16	16	19	30	9	20	40	53	40
LINEATION	StrLIN	StrLIN							
DIP_DIREC	268	292							
DIP	10	15							
FA DIP_DIR									
FA DIP									
AP DIP-DIR									
AP DIP									
LAT_N_S	250664,47	250301,6	249790,58	249545,42	249726,54	249774,07	250216,82	250216,82	250277,65
LON_E_W	4242463	4242537,7	4242645,9	4242685	4242881,9	4242859,2	4242706,6	4242706,6	4242663,8
ALTITUDE	322	396	502	511	431	434	400		366
Probennr									

Nummer	A1	A1	A2	A2	A2	A2	A2	A2	A2
LocNr.	**A37**	**A37**	**A02**	**A03**	**A05**	**A06**	**A06**	**A14**	**A15**
Lithology	M	M	K	K	M	M	K	M	M
PLANE	S0	S1	S0	S0	S0		S0	S0	S0
DIP_DIREC	281	279	272	220	210		300	212	314
DIP	34	66	45	24	35		35	25	15
LINEATION				StrLin		StrLin	StrLin		StrLin
DIP_DIREC				282		302	258		273
DIP				5		13	25		5
FA DIP_DIR									
FA DIP									
AP DIP-DIR									
AP DIP									
LAT_N_S	249483,22	249483,22	250023,67	249967,4	249897,59	249866,35	249866,35	247921,74	247766,07
LON_E_W	4241088,2	4241088,2	4244213,7	4244217	4244235,2	4244241,3	4244241,3	4242664,5	4242499,2
ALTITUDE	112		144	125	142	137		17	23
Probennr									

Nummer	A2	A2	A5	A5	A5	A5	A5	A5	A5
LocNr.	**A16**	**A20**	**A01**	**A02**	**A02**	**A03**	**A03**	**A06**	**A07**
Lithology	M	M	M	M	M	M		M	M
PLANE	S0	S0	S0	S0	S1	S0	S1	Speleo	S0
DIP_DIREC	268	276	278	268	235	264	268	242	300
DIP	25	25	43	30	41	41	51	90	35
LINEATION	StrLin	StrLin		StrLin		StrLin		StrLin	StrLin
DIP_DIREC	273	302		272		302		50	272
DIP	5	25		40		21		85	32
FA DIP_DIR									
FA DIP									
AP DIP-DIR									
AP DIP									
LAT_N_S	247613,51	247176,04	249510,5	249496,36	249496,36	248833,23	248833,23	248611,65	248563,07
LON_E_W	4242318,5	4240803,5	4240250,1	4240229,2	4240229,2	4239676,8	4239676,8	4239246,3	4238869,8
ALTITUDE	42	81	4	4		4		25	35
Probennr									A02/21

Nummer	A5	A5	A5	A5	A5	A5	A5	A5	A5
LocNr.	**A08**	**A08**	**A09**	**A09**	**A11**	**A12**	**A12**	**A12**	**A13**
Lithology	M		M	M	K	M	M	M	M
PLANE	S0	S0	S0	S1	S0	Kat	Kat	S0	S0
DIP_DIREC			266	308	156	300	310	306	308
DIP			44	38	30	78	6	66	42
LINEATION					CrenLin			StrLin	StrLin
DIP_DIREC					15			262	259
DIP					6			54	19
FA DIP_DIR									
FA DIP									
AP DIP-DIR	254	268							
AP DIP	61	39							
LAT_N_S	248502,01	248502,01	247901,73	247901,73	247279,51	247063,58	247063,58		247113,15
LON_E_W	4238599,2	4238599,2	4238287,9	4238287,9	4238229,3	4238520,9	4238520,9		4239257,3
ALTITUDE	13		46		39	40	40		6
Probennr						A03/21			

Nummer	A5	A5	A5	A5	A5	A5	A6	A6	A6
LocNr.	**A14**	**A14**	**A15**	**A16**	**A18**	**A18**	**A01**	**A01**	**A02**
Lithology	K	K	K	K	M	M	K	K	K
PLANE	S0	S1	S0	S0	S0	S1	S0	S1	S0
DIP_DIREC	321	279	330	329	270	258	291	200	206
DIP	44	52	29	21	46	68	32	22	37
LINEATION			StrLin	CrenLin	StrLin		CrenLin		
DIP_DIREC			282	356	270		222		
DIP			21	26	30		30		
FA DIP_DIR			14					200	
FA DIP			30					22	
AP DIP-DIR			44						
AP DIP			35						
LAT_N_S	247074,46	247074,46	247059,1	246934,17	247278,59	247278,59	247509,19	247509,19	247509,26
LON_E_W	4239247,1	4239247,1	4239243	4239270,3	4240097,4	4240097,4	4250840,6	4250840,6	4250987,9
ALTITUDE	-7		-13	2	99				160
Probennr		A04/21	A05/21						

Nummer	A6	A6	A6	A6	A6	A7	A7	A7	A7
LocNr.	**A03**	**A04**	**A05**	**A08**	**A10**	**A03**	**A04**	**A04**	**A06**
Lithology	K	K	F	M	M	M	K	M	M
PLANE	S0	S0	S0	S0	S0	S0	S0	S0	S0
DIP_DIREC	299	302	359	61	211	250	212	212	268
DIP	35	25	35	4	35	3	21	21	24
LINEATION		CrenLin				StrLin	StrLin		
DIP_DIREC		226				242	248		
DIP		8				21	6		
FA DIP_DIR	222	226	298						
FA DIP	25	8	11						
AP DIP-DIR	286	220	10						
AP DIP	40	6	50						
LAT_N_S	247470,28	247628,29	245212,19	245248,49	245137,08	249155,35	249080,99	249080,99	248910,23
LON_E_W	4251083,7	4251194,2	4247069,3	4247617,3	4247636,3	4246298,6	4246383,7	4246383,7	4246470,3
ALTITUDE	141	157	522	556	594	205	226		278
Probennr									

Nummer	A7	A7	A7	A7	A7	A7	A7	A7	A7
LocNr.	**A07**	**A08**	**A09**	**A11**	**A13**	**A14**	**A17**	**A18**	**A19**
Lithology	M	M	M	M	F	F	M	M	M
PLANE	S0	S0	S0	S0	S0	S0	S0	S0	S0
DIP_DIREC	224	216	225	239	252	212	279	242	264
DIP	40	35	26	29	30	26	21	15	20
LINEATION	StrLin	StrLin		StrLin					
DIP_DIREC	268	238		258					
DIP	4	31		33					
FA DIP_DIR									
FA DIP									
AP DIP-DIR									
AP DIP									
LAT_N_S	248938,57	248964,4	248954,81	248932,52	248873,09	248732,61	249242,38	249485,16	249543,38
LON_E_W	4246492,3	4246490,1	4246567	4246666,1	4246873,7	4246954,3	4246789,7	4246517,5	4246481,8
ALTITUDE	282	283	333	370	321	279	292	283	278
Probennr		A07/21							

Nummer	A7	A7	A7	A7	A7	A7	A7	A7	A8
LocNr.	**A20**	**A21**	**A21**	**A22**	**A24**	**A24**	**A25**	**A26**	**A01**
Lithology	M	M	M	K	K	K	M	K	K
PLANE	S0	S0	S1	S0	S0	S1	S0	S0	S0
DIP_DIREC	224	260	254	296	280	258	242	260	116
DIP	34	21	35	40	23	41	25	24	45
LINEATION	StrLin						StrLin	CrenLin	
DIP_DIREC	251						246	257	
DIP	33						12	21	
FA DIP_DIR								342	
FA DIP								21	
AP DIP-DIR								69	
AP DIP								52	
LAT_N_S	249514,35	249485,12	249485,12	249514,79	249517,22	249517,22	249479,1	249433,76	242478,25
LON_E_W	4246381,1	4246367	4246367	4246333,2	4246310,1	4246310,1	4246308,3	4246251,6	4247282,8
ALTITUDE	249	244		231	230		198	204	23
Probennr	A08/21	A09/21			A10/21				

Nummer	A8	A8	A8	A8	A8	A8	A8	A8	A8
LocNr.	**A02**	**A03**	**A03**	**A04**	**A05**	**A06**	**A07**	**A08**	**A08**
Lithology	K	K	K	K	K	M	M	M	M
PLANE	S0	S0	S0	S0	S0	S0	S0	S0	S1
DIP_DIREC	112	144		162	241	202	194	198	208
DIP	40	35		34	12	28	40	36	52
LINEATION					StrLin				
DIP_DIREC					246				
DIP					26				
FA DIP_DIR		240							
FA DIP		80							
AP DIP-DIR		238	230						
AP DIP		22	45						
LAT_N_S	242428,84	242359,87	242359,87	242236,41	242158,01	242092,88	241965,28	241791,28	241791,28
LON_E_W	4247264,7	4247236,9	4247236,9	4247196,4	4247158,4	4247067,3	4246988	4246976,3	4246976,3
ALTITUDE	19	44		46	55	50	69	103	
Probennr									

Nummer	A8	A8	A8	A8	A8	A8	A8	A9	A9
LocNr.	**A09**	**A10**	**A10**	**A10**	**A11**	**A11**	**A12**	**A01**	**A01**
Lithology	M	M	M	M	M	M	M	M	M
PLANE	S0	S0	S1	S0	S0	S0	S0	S0	S0
DIP_DIREC	202	197	162	252	318	244	166	62	
DIP	21	28	29	16	20	20	24	18	
LINEATION					StrLin			StrLin	
DIP_DIREC					254			281	
DIP					16			10	
FA DIP_DIR								268	
FA DIP								11	
AP DIP-DIR								194	42
AP DIP								20	22
LAT_N_S	241480,41	241512,36	241512,36	241512,36	241375,88	241375,88	242070,14	241361,21	241361,21
LON_E_W	4246918,3	4246858,6	4246858,6	4246858,6	4246788,8	4246788,8	4247040,4	4246620,7	4246620,7
ALTITUDE	149	142			156		45	135	
Probennr					A11/21				

Nummer	A9	A9	A9	A9	A9	A9	A9	A9	A9
LocNr.	**A01**	**A01**	**A02**	**A03**	**A04**	**A05**	**A07**	**A07**	**A07**
Lithology	M	M	M	M	M	M	K	M	M
PLANE	S0	S0	S0	S0	S0	S0	S0	S0	S1
DIP_DIREC			42	74	26	38	232	232	238
DIP			25	21	42	25	15	15	31
LINEATION				StrLin		StrLin	StrLin		
DIP_DIREC				130		121	266		
DIP				4		6	6		
FA DIP_DIR	272								
FA DIP	18								
AP DIP-DIR	172	100							
AP DIP	25	16							
LAT_N_S	241361,21	241361,21	241231,19	241182,69	241041,07	240911,57	240670,47	240670,47	240670,47
LON_E_W	4246620,7	4246620,7	4246548,1	4246566,6	4246609,9	4246646,2	4246867,2	4246867,2	4246867,2
ALTITUDE			124	130	106	94	17		
Probennr							A12/21		

Nummer	A9	A9	A9	A9	A9	A10	A10	A10	A10
LocNr.	**A08**	**A09**	**A13**	**A15**	**A18**	**A02**	**A03**	**A04**	**A05**
Lithology	K	K	M	F	F	M	M	M	M
PLANE	S0	S0	S0	S0	S0	S0	S0	S0	S0
DIP_DIREC	288	262	324	256	214	308	233	288	279
DIP	12	15	12	19	70	10	26	21	36
LINEATION	StrLin	StrLin	StrLin					StrLin	
DIP_DIREC	274	284	270					277	
DIP	6	4	8					43	
FA DIP_DIR									
FA DIP									
AP DIP-DIR									
AP DIP									
LAT_N_S	240575,09	240568,57	240196,63	240091,64	239976,4	248032,72	247961,94	247563,34	246637,48
LON_E_W	4246993	4247048,6	4247347,5	4247329,4	4247009,5	4244445	4244701,5	4245004,4	4245169,5
ALTITUDE	-4	5	-3	12	-7	188	118	42	9
Probennr		A13/21	A14/21						

Nummer	A10	A10	A10	A10	A10	A10	A10	A11	A11
LocNr.	**A05**	**A08**	**A09**	**A11**	**A12**	**A13**	**A15**	**A01**	**A02**
Lithology	M	M	K	M	M	K	M	K	M
PLANE	S1	S0	S0	S0	S0	S0	S0	S0	S0
DIP_DIREC	295	269	132	194	272	265	189	290	44
DIP	44	10	29	25	20	17	46	45	5
LINEATION									StrLin
DIP_DIREC									316
DIP									3
FA DIP_DIR			221						
FA DIP			25						
AP DIP-DIR									
AP DIP									
LAT_N_S	246637,48	245630,77	245281,5	244950,1	244405,74	244372,1	244444,93	240864,84	240801,6
LON_E_W	4245169,5	4245796	4245702,6	4245646,3	4245882,6	4245572	4245796,2	4246608,1	4246603,8
ALTITUDE		30	9	49	75	3	36	116	98
Probennr			A15/21			A16/21			

Nummer	A11	A11	A11	A11	A11	A11	A11	A11	A11
LocNr.	**A06**	**A08**	**A10**	**A11**	**A13**	**A14**	**A14**	**A14**	**A14**
Lithology	M	K	M	K	F	K	K	K	
PLANE	S0	S0	S0	S0	S0	S0	S0	S1	S1
DIP_DIREC	283	106	216	252	4	334	330	348	
DIP	5	29	20	36	25	20	16	53	
LINEATION		StrLin	StrLin	CrenLin					
DIP_DIREC		66	246	249					
DIP		11	6	41					
FA DIP_DIR							262	259	275
FA DIP							26	33	30
AP DIP-DIR							317	326	
AP DIP							17	38	
LAT_N_S	241082,58	240962,06	240981,04	240993,85	244852,91	244821,48	244821,48	244821,48	244821,48
LON_E_W	4246231,7	4246204,4	4246002,2	4246161,2	4248749	4248792,8	4248792,8	4248792,8	4248792,8
ALTITUDE	122	67	52	90	393	405			
Probennr			A17/21	A18/21					

Nummer	A11	A11	A11	A11	A11	A11	A11	A11	A11
LocNr.	**A15A**	**A16**	**A17**	**A18**	**A18A**	**A18A**	**A20A**	**A20A**	**A21**
Lithology	F	M	K	K	K	K	F	F	F
PLANE	S0	S0	S0	S0	S0	S0	S0	S0	S0
DIP_DIREC	350	248	294	180	350	346	146	143	335
DIP	21	14	9	36	18	4	35	11	11
LINEATION	StrLin			StrLin			StrLin		StrLin
DIP_DIREC	72			81			243		58
DIP	23			1			1		19
FA DIP_DIR					252				
FA DIP					24				
AP DIP-DIR					209				
AP DIP					44				
LAT_N_S	244749,76	244375,6	244615,78	244666,14	244658,86	244658,86	244602,62	244602,62	244692,78
LON_E_W	4248912,1	4250179,5	4249982,6	4249857,4	4249876,2	4249876,2	4249354,6	4249354,6	4249273,4
ALTITUDE	423			534	529		503		449
Probennr			A19/21						

Nummer	A11	A11	A11	A11	A11	A11	A11	A11	A11
LocNr.	**A22**	**A22**	**A22**	**A22**	**A23**	**A23**	**A23**	**A26**	**A27**
Lithology	K	K	K	Pebble	M	M	M	M	M
PLANE	S0	S0	S0	S0	S0	S0	S0	S0	S0
DIP_DIREC	120	70	70	146	233	216	196	238	296
DIP	12	15	21	21	19	26	23	9	17
LINEATION	StrLin								
DIP_DIREC	64								
DIP	11								
FA DIP_DIR									
FA DIP									
AP DIP-DIR									
AP DIP									
LAT_N_S	244591,66	244591,66	244591,66	244591,66	244465,05	244465,05	244465,05	244931,26	244965,38
LON_E_W	4249243,6	4249243,6	4249243,6	4249243,6	4249168,4	4249168,4	4249168,4	4248789,4	4248731,2
ALTITUDE	503				515			346	321
Probennr									

Nummer	A11	A11	A11	A11	A11	A11	A11	A11	A11
LocNr.	**A27**	**A27**	**A28**	**A28**	**A28**	**A29**	**A29**	**A29**	**A29**
Lithology	M	M	M	M	M	M	M	M	M
PLANE	Fault	Fault	S0	Fault	Fault	S0	S0	Fault	Fault
DIP_DIREC	177	322	238	350	170	248	255	305	142
DIP	66	30	17	50	59	17	14	55	52
LINEATION									
DIP_DIREC									
DIP									
FA DIP_DIR									
FA DIP									
AP DIP-DIR									
AP DIP									
LAT_N_S	244965,38	244965,38	245024,1	245024,1	245024,1	245062,74	245062,74	245062,74	245062,74
LON_E_W	4248731,2	4248731,2	4248623,6	4248623,6	4248623,6	4248398,4	4248398,4	4248398,4	4248398,4
ALTITUDE	321	321	348	348	348	313	313	313	313
Probennr						A22/21			

Nummer	A12	A12	A12	A12	A12	A12	A12	A12	A12
LocNr.	**A02**	**A03**	**A04**	**A06**	**A07**	**A09**	**A10**	**A11**	**A12**
Lithology	F	M	M	K	F	K	F	F	K
PLANE	S0	S0	S0	S0	S0	S0	S0	S0	S0
DIP_DIREC	316	252	244	250	194	244	231	305	263
DIP	21	21	16	3	18	14	21	3	15
LINEATION	StrLin		StrLin						StrLin
DIP_DIREC	241		243						270
DIP	6		13						9
FA DIP_DIR									
FA DIP									
AP DIP-DIR									
AP DIP									
LAT_N_S	246536,59	246548,22	246994,09	247089,93	247072,87	247044,62	247111,08	247145,23	247184,12
LON_E_W	4249445,3	4249425,6	4248900,7	4248846,3	4248776,5	4248693	4248786,8	4248899,5	4248937,2
ALTITUDE	140	142	193	179	199	111	201	196	232
Probennr								A20/21	

Nummer	A12	A12	A12	A12	A12	A12	A13	A13	A13
LocNr.	**A12**	**A13**	**A13**	**A14**	**A16**	**A17**	**A01**	**A01**	**A02**
Lithology	K	F	F	F	K	K	K	K	K
PLANE	S1	S0	Fault	S0	S0	S0	S0	Fault	S0
DIP_DIREC	266	279	242	279	330	267	330	260	233
DIP	31	13	29	30	7	27	29	27	47
LINEATION						StrLin	StrLin		
DIP_DIREC						225	230		
DIP						20	18		
FA DIP_DIR									
FA DIP									
AP DIP-DIR									
AP DIP									
LAT_N_S	247184,12	247248,05	247248,05	247367,79	246913,56	246848,48	247718,82	247718,82	247650,12
LON_E_W	4248937,2	4248880,6	4248880,6	4248795,8	4248403,2	4248367,3	4250965,5	4250965,5	4250562
ALTITUDE		242	242	244	237	250	80	80	52
Probennr									

Nummer	A13	A13	A13	A13	A13	A13	A13	A13	A13
LocNr.	**A02**	**A03**	**A04**	**A06**	**A07**	**A09**	**A10**	**A10**	**A11**
Lithology	K	M	K	F	M	M	K	K	K
PLANE	S0	S0	S0	S0	S0	S0	S0	S1	S0
DIP_DIREC	246	191	253	298	18	291	314	353	321
DIP	59	22	49	18	37	18	25	34	21
LINEATION				StrLin			CrenLin		
DIP_DIREC				250			266		
DIP				21			7		
FA DIP_DIR					19				
FA DIP					38				
AP DIP-DIR									
AP DIP									
LAT_N_S	247650,12	247798,98	247931,3	248121,34	248030,2	247785,63	247659,17		247643,07
LON_E_W	4250562	4250285	4250158,2	4249406,9	4248520,1	4248482,6	4248515,1		4248582,1
ALTITUDE		26	16	46	36	81	102		87
Probennr							A24/21		

Nummer	A13	A13	A13	A13	A13	A13	A13	A13	A13
LocNr.	**A12**	**A12**	**A12**	**A13**	**A13**	**A14**	**A14**	**A15**	**A17**
Lithology	K	K	K	K	K	K	K	K	M
PLANE	S0	S0	QtzBoud	S0	S1	S0	S1	QtzPeb	S0
DIP_DIREC	259	273	271	286	262	260	234	342	216
DIP	7	31	32	25	22	14	44	31	24
LINEATION	StrLin			StrLin		StrLin			
DIP_DIREC	270			260		232			
DIP	7			21		8			
FA DIP_DIR									
FA DIP									
AP DIP-DIR									
AP DIP									
LAT_N_S	247588,69	247588,69	247588,69	247455,31	247455,31	247338,55	247338,55	247350,86	247506,95
LON_E_W	4248653,1	4248653,1	4248653,1	4248598,6	4248598,6	4248421,1	4248421,1	4248185,8	4248062,8
ALTITUDE	160			139		191		152	147
Probennr						A25/21			

Nummer	A14	A14	A14	A14	A14	A14	A14	A14	A14
LocNr.	**A01**	**A03**	**A05**	**A06**	**A07**	**A07**	**A08**	**A09**	**A09**
Lithology	F	K	F	K	M	M	K	M	M
PLANE	S0	S0	S0	S0	S0	S1	S0	S0	S1
DIP_DIREC	12	30	344	51	194	193	118	33	173
DIP	15	27	44	7	13	33	9	19	55
LINEATION	StrLin	StrLin	StrLin					StrLin	
DIP_DIREC	93	60	52					55	
DIP	2	28	3					14	
FA DIP_DIR									
FA DIP									
AP DIP-DIR									
AP DIP									
LAT_N_S	241532,66	241764,71	242109,82	242437,88	242223,49	242223,49	242230,39	242259,42	242259,42
LON_E_W	4246596,2	4246471,5	4246384,4	4246317	4246145,5	4246145,5	4246024,5	4245982,5	4245982,5
ALTITUDE	185	190	216	216	164		112	111	
Probennr									

Nummer	A14	A14	A14	A14	A14	A14	A14	A14	A14
LocNr.	**A10**	**A15**	**A16**	**A17**	**A17**	**A19**	**A20**	**A21**	**A21**
Lithology	F	F	K	K	K	M	M	M	M
PLANE	S0	S0	S0	S0	S0	S0	S0	S0	S0
DIP_DIREC	343	205	224	215	257	222	256	231	214
DIP	8	47	65	58	51	52	70	33	62
LINEATION									
DIP_DIREC									
DIP									
FA DIP_DIR									
FA DIP									
AP DIP-DIR									
AP DIP									
LAT_N_S	242285,91	243907,59	243898,87	243875,03	243875,03	243777,01	243616,04	242945,48	242945,48
LON_E_W	4245943,1	4246156,8	4246132,8	4246090,3	4246090,3	4245933,5	4245814,6	4245791,7	4245791,7
ALTITUDE	122	-33	-6	21		14	18	40	
Probennr			A26/21			A27/21			

Nummer	A14	A14	A14	A14	A14	A14	A14	A14	A14
LocNr.	**A22**	**A22**	**A24**	**A26**	**A30**	**A32**	**A34**	**A34**	**A34**
Lithology	M	M	F	M	K	K	K	K	K
PLANE	S0	S0	S0	S0	S0	S0	S0	S0	S0
DIP_DIREC	204		196	191	207	183	197		
DIP	30		39	40	19	31	12		
LINEATION	StrLin	StrLin	StrLin		CrenLin				
DIP_DIREC	274	267	260		230				
DIP	17	32	24		20				
FA DIP_DIR							125	137	52
FA DIP							7	3	8
AP DIP-DIR							228	230	320
AP DIP							12	4	10
LAT_N_S	242777,37	242777,37	242665,1	242541,66	242268,85	242325,96	242352,2	242352,2	242352,2
LON_E_W	4245839,1	4245839,1	4245859,2	4245976,3	4245817,4	4245832,5	4245952,6	4245952,6	4245952,6
ALTITUDE	70		78	64	52	51	136		
Probennr									

Nummer	A14	A15	A15	A15	A15	A15	A15	A15	A15
LocNr.	**A38**	**A01**	**A03**	**A04**	**A06**	**A08**	**A09**	**A11**	**A12**
Lithology	K	F	M	K	M	M	M	M	F
PLANE	S0	S0	S0	S0	S0	S0	S0	S0	S0
DIP_DIREC	237	198	208	201	200	257	239	268	257
DIP	34	40	40	11	30	10	7	11	18
LINEATION						StrLin			StrLin
DIP_DIREC						265			254
DIP						16			9
FA DIP_DIR						330	347		
FA DIP						7	5		
AP DIP-DIR						250	262		
AP DIP						4	1		
LAT_N_S	241967,63	241366,45	240614,11	240566,99	240489,19	240509,24	240415,33	240151,52	240019,63
LON_E_W	4246232,1	4246584,7	4246595,2	4246564	4246305,7	4246210,6	4246036,6	4246031,1	4246186,3
ALTITUDE	178	112	97	109	95	72	8	18	9
Probennr									

Nummer	A15	A15	A15	A15	A15	A15	A15	A15	A15
LocNr.	**A13**	**A14**	**A15**	**A15**	**A17**	**A18**	**A19**	**A20**	**A22**
Lithology	M	M	F	F	K	K	K	K	K
PLANE	S0	S0	S0	S0	S0	S0	S0	S0	S0
DIP_DIREC	9	342	28	16	3	13	30	332	195
DIP	14	10	16	12	14	8	16	23	31
LINEATION			StrLin						
DIP_DIREC			88						
DIP			4						
FA DIP_DIR			87	86		98			
FA DIP			6	17		10			
AP DIP-DIR			16	43		46			
AP DIP			3	17		14			
LAT_N_S	240076,32	239875,04	239900,65	239900,65	239851,53	239841,47	239825,83	240137,08	241702,44
LON_E_W	4246305,2	4246398,3	4246709,4	4246709,4	4246638	4246627,4	4246598,4	4246381,9	4246341,6
ALTITUDE	-7	10	-5		-20	23	8	53	174
Probennr		A29/21	A30/21						

A.2. XYZ-data

Nummer	A1	A1	A1	A2	A2
LocNr.	A01	A14	A30	A01	A02
X	14	22	11	57	22
Y					
Z	2,5	2	4	11	2
Area	Southern	Southern	Southern	Southern	Southern
LAT_N_S	249601,137	249953,257	249774,074	250053,987	250023,668
LON_E_W	4240388,6	4241927,6	4242859,25	4244217,51	4244213,68
ALTITUDE	21	185	434	141	144
Nummer	A2	A2	A2	A5	A5
LocNr.	A06	A06	A07	A11	A15
X	8	118	44	11	100
Y					88
Z	2	8	5	3	2
Area	Southern	Southern	Southern	Southern	Southern
LAT_N_S	249866,35	249866,35	249826,291	247279,513	247059,095
LON_E_W	4244241,32	4244241,32	4244242,34	4238229,32	4239242,98
ALTITUDE			109	39	-13
Nummer	A7	A7	A7	A7	A8
LocNr.	A22	A24	A24	A26	A02
X	24	35	52	45	24
Y			38	11	
Z	4	52	5		5
Area	Middle	Middle	Middle	Middle	Western
LAT_N_S	249514,789	249517,224	249517,224	249433,758	242428,841
LON_E_W	4246333,19	4246310,11	4246310,11	4246251,6	4247264,69
ALTITUDE	231	230		204	19
Nummer	A10	A11	A13	A13	A13
LocNr.	A09	A18	A01	A13	A13
X	95	75	167	159	88
Y		50			
Z	8	15	10	6	4
Area	Middle	Middle	Middle	Middle	Middle
LAT_N_S	245281,497	244666,137	247718,822	247455,309	247455,309
LON_E_W	4245702,56	4249857,38	4250965,47	4248598,61	4248598,61
ALTITUDE	9	534	80	139	